1

Hydrogen Co-deposition Effects on the Structure of Electrodeposited Copper

Nebojša D. Nikolić[1] and Konstantin I. Popov[1,2]

[1] *ICTM-Institute of Electrochemistry, University of Belgrade, Njegoševa 12, Belgrade, Serbia*
[2] *Faculty of Technology and Metallurgy, University of Belgrade, Karnegijeva 4, Belgrade, Serbia*

I. INTRODUCTION

The creation of open porous structures with an extremely high surface area is of great technological significance because such structures are ideally suited for electrodes in many electrochemical devices, such as fuel cells, batteries, and chemical sensors.[1] The open porous structure enables the fast transport of gases and liquids, while the extremely high surface area is desirable for the evaluation of electrochemical reactions. The electrodeposition technique is very suitable for the preparation of such structures because it is possible to control the number, distribution, and pore size in these structures by the choice of appropriate electrolysis parameters.

These metal structures can be formed in both potentiostatic and galvanostatic regimes of electrolysis and their formation are always accompanied by strong hydrogen co-deposition. Hydrogen evolution is the second reaction which occurs at the cathode during electrodeposition processes from aqueous solutions; in some cases it can be

S.S. Djokić (ed.), *Electrodeposition: Theory and Practice*,
Modern Aspects of Electrochemistry 48, DOI 10.1007/978-1-4419-5589-0_1,

ignored while in other cases it cannot.[2] Co-deposition of hydrogen during chromium electroplating is the best documented system,[3,4] because the cathode current efficiency for chromium electrodeposition is 10–25%. Generally, the effect of hydrogen co-deposition during metal electrodeposition processes can be manifested through:[2]

1. Hydrogen absorption which occurs in the substrate metal as H atoms, not H_2 molecules, but may gather as molecule bubbles in voids or vacancies, thus leading to hydrogen embrittlement.
2. Hydrogen bubbles which cling to the surface in an adsorbed state; this leads to the growth of pores as the deposition continues around the bubbles before they are released.
3. Hydrogen bubble evolution can provide a stirring effect and lead to a substantial bubble raft at the free surface of the solution.

The most often employed electrolytes for the electrodeposition of copper are those based on aqueous solutions of sulfuric acid (H_2SO_4) and cupric sulfate ($CuSO_4$).[5] The main species present in aqueous sulfuric acid solutions containing Cu(II) are: bisulfate ions (HSO_4^-), cupric ions (Cu^{2+}), aqueous cupric sulfate ($CuSO_{4(aq)}$), hydrogen ions (H^+), and sulfate ions (SO_4^{2-}).[6–8] In an aqueous solution of sulfuric acid and cupric sulfate, two weak electrolytes, HSO_4^- and $CuSO_{4(aq)}$, are formed according to the following reactions:

$$H^+ + SO_4^{2-} \rightleftarrows HSO_4^- \quad (1)$$

$$Cu^{2+} + SO_4^{2-} \rightleftarrows CuSO_{4(aq)} \quad (2)$$

Pitzer's model[9] was used to calculate the ionic equilibrium in the $CuSO_4$–H_2SO_4–H_2O system over a wide range of concentrations and temperatures.[8] Using Pitzer's model, the relative concentrations of hydrogen ions (H^+) as a function of the total copper concentration and solution acidity were calculated, and this dependence is presented in Fig. 1. From Fig. 1 it can be clearly seen that increasing the copper concentration produces a sharp decrease in the hydrogen ion concentration, while increasing the concentration of sulfuric acid produces an increase in the hydrogen ion concentration.

According to (1) and (2), the addition of sulfuric acid to the solution decreases the concentration of free sulfate ions due to the

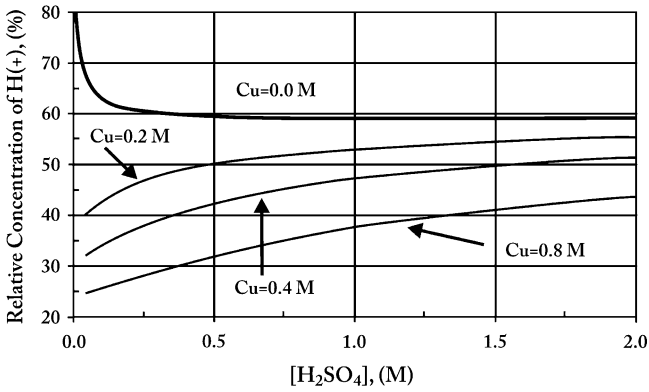

Figure 1. Relative concentration of hydrogen ions as function of sulfuric acid and total copper concentrations, at 25°C ($C_{RH+} = [H^+]/[H_T]$). (Reprinted from Ref. [8] with permission from Elsevier).

formation of bisulfate ions. The addition of cupric sulfate to the solution increases the concentration of bisulfate ions and decreases the concentration of hydrogen ions.

In the case of copper electrodeposition,[10] as opposed to other metals such as nickel and cobalt,[11,12] there are well-defined ranges of current densities and overpotentials without and with hydrogen co-deposition. The beginning of the hydrogen evolution reaction, as the second reaction, corresponds to some overpotential belonging to the plateau of the limiting diffusion current density, being higher than the critical overpotential for the initiation of dendritic growth and lower than that for instantaneous dendritic growth.[13] Increasing the overpotential intensifies the hydrogen evolution reaction and at some overpotential outside the plateau of the limiting diffusion current density, hydrogen evolution becomes vigorous enough to change the hydrodynamic conditions in the near-electrode layer. This offers the possibility of detailed investigations and comparison of the morphologies of copper, and consequently, of any other metals, obtained without and with hydrogen co-deposition.

In the case of copper, electrodeposition at low overpotentials produces large grains with relatively well-defined crystal shapes. Further increasing the overpotential leads to the formation of cauliflower-like and carrot-like protrusions, and finally, dendritic deposits are formed in the absence of strong hydrogen co-deposition.[13]

Strong hydrogen co-deposition leads to a mixing of the solution and changes the mass transfer limitations at an electrode surface. At the same time, the evolved hydrogen bubbles exert substantial effects on mass and heat transfer, limiting current density and ohmic resistance,[14–16] as well as on the morphology of the deposit, leading to the formation of open porous structures with an extremely high surface area.[1,10,17–19]

Electrodeposition of copper under conditions of a vigorous hydrogen co-deposition is of high technological significance, because open porous structures of copper with an extremely high surface area are suitable for the construction of nanocomposite anodes (consisting of Cu and CeO_2) for solid oxide fuel cells.[1] Also, copper shows a high activity for nitrate ion reduction,[20] as well as for a reaction in which nitrate is reduced to ammonia in high yield in aqueous acidic perchlorate and sulfate media.[21]

Bearing in mind the great practical significance of copper deposits obtained under the conditions of hydrogen co-deposition, as well as the fact that detailed investigations at high current densities and overpotentials have been performed only from the point of view of the formation of metal powders,[13,22–25] a better understanding of the effect of hydrogen evolution on the electrodeposition of copper at high overpotentials is necessary.

The morphology of electrodeposited copper in the presence of vigorous hydrogen evolution was described recently,[1] and the mechanism of the formation of this type of morphology was established by Nikolić et al.[10]

The aim of this chapter was to give comprehensive treatment of the morphology of copper electrode posited at high overpotentials, especially in the presence of hydrogen co-deposition, obtained in the potentiostatic conditions from different electrolytes and at different temperatures.

II. THE CONCEPT OF "THE EFFECTIVE OVERPOTENTIAL"

1. The Definition of the Concept and Mathematical Model

The polarization curve for copper electrodeposition from 0.15 M $CuSO_4$ in 0.50 M H_2SO_4 is shown in Fig. 2. The average current efficiencies for hydrogen evolution reaction, $\eta_{av}(H_2)$, in potentiostatic

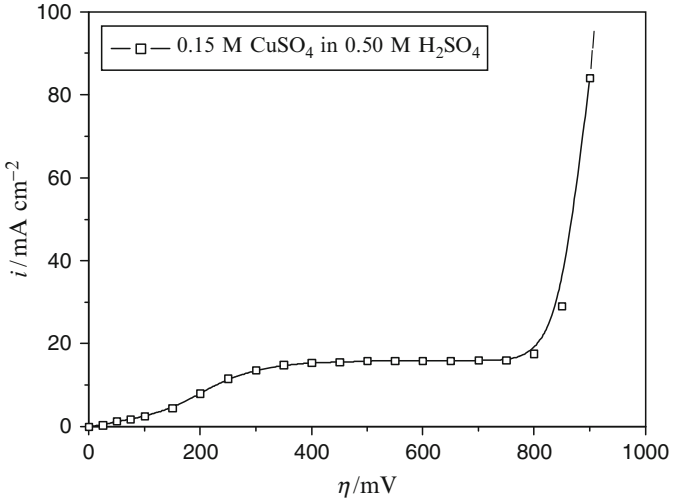

Figure 2. Polarization curve for the cathodic process of copper deposition from 0.15 M $CuSO_4$ in 0.50 M H_2SO_4. Temperature: 18.0 ± 1.0°C. (Reprinted from Ref. [10] with permission from Elsevier).

deposition are derived from the dependences of the current of copper electrodeposition on time and the dependences of the volume of the evolved hydrogen on time[10] using procedure described in Ref. [26]

The average current efficiency for hydrogen evolution reaction at an overpotential of 700 mV was very small (near 2.0%),[10] and at lower overpotentials it even cannot be observed. The average current efficiency for the hydrogen evolution at an overpotential of 800 mV was 10.8%, while at an overpotential of 1,000 mV was 30.0%.[10] The critical overpotential for the beginning of the hydrogen evolution can be estimated to be about 680 mV.[10]

The morphologies of copper electrodeposits obtained potentiostatically, onto vertical stationary copper wire electrodes previously covered by copper thin films[10] from a copper solution containing 0.15 M $CuSO_4$ in 0.50 M H_2SO_4, at a temperature of 18.0 ± 1.0°C in different hydrogen co-deposition conditions are shown in Figs. 3–10.

The deposits obtained at an overpotential of 550 mV with different quantities of electricity are shown in Figs. 3–6. At this overpotential, there is no hydrogen co-deposition at all. The deposit obtained with a quantity of electricity of 2.5 mA h cm^{-2} is shown

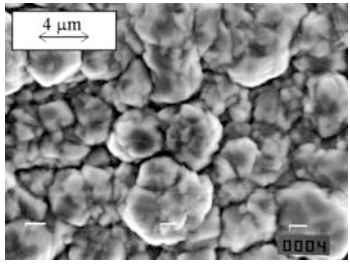

Figure 3. Copper deposit obtained at an overpotential of 550 mV. Quantity of electricity: 2.5 mA h cm^{-2}. (Reprinted from Ref.[10] with permission from Elsevier).

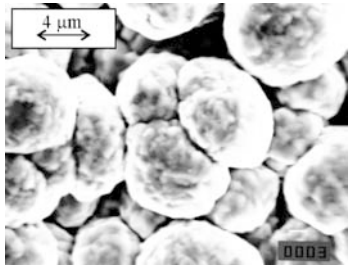

Figure 4. Copper deposit obtained at an overpotential of 550 mV. Quantity of electricity: 5.0 mA h cm^{-2}. (Reprinted from Ref.[10] with permission from Elsevier).

in Fig. 3. The surface film is completed, the grains grown by electrodeposition on the initially formed nuclei practically touch each other and there is no new nucleation on already existing grains. The difference in size between grains can also be observed. This is due to the fact that the nucleation does not occur simultaneously over the whole cathode surface, but it is a process extended in time, so that crystals generated earlier may be considerably larger in the size than ones generated later. These differences increase with an increased quantity of electrodeposited metal, what can be seen from Fig. 4 presenting the copper deposit obtained with a quantity of

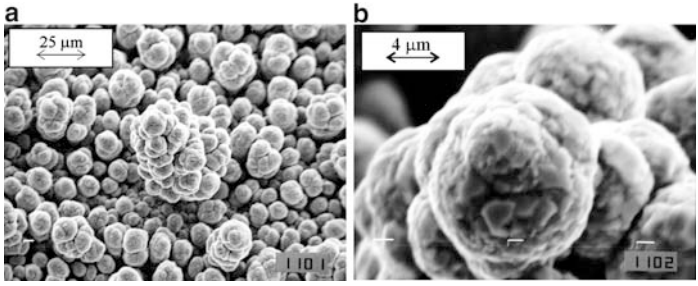

Figure 5. Copper deposit obtained at an overpotential of 550 mV: (**a**) cauliflower-like structure, and (**b**) the detail from Fig. 5a. Quantity of electricity: 10 mA h cm^{-2}. (Reprinted from Ref. [10] with permission from Elsevier).

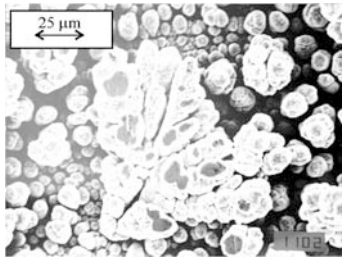

Figure 6. Copper deposit obtained at an overpotential of 550 mV. Quantity of electricity: 20 mA h cm^{-2}. (Reprinted from Ref. [17] with permission from Elsevier).

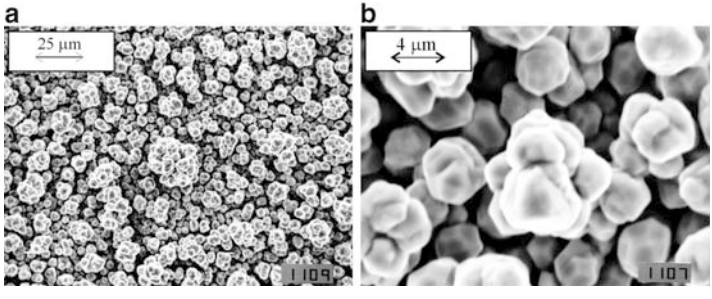

Figure 7. Copper deposit obtained at an overpotential of 700 mV: (**a**) cauliflower-like structure, and (**b**) the detail from Fig. 7a. Quantity of electricity: 2.5 mA h cm^{-2}. (Reprinted from Ref. [10] with permission from Elsevier).

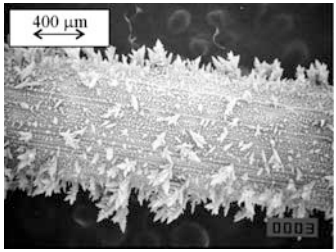

Figure 8. Copper deposit obtained at an overpotential of 700 mV. Quantity of electricity: 5.0 mA h cm^{-2}. (Reprinted from Ref. [10] with permission from Elsevier).

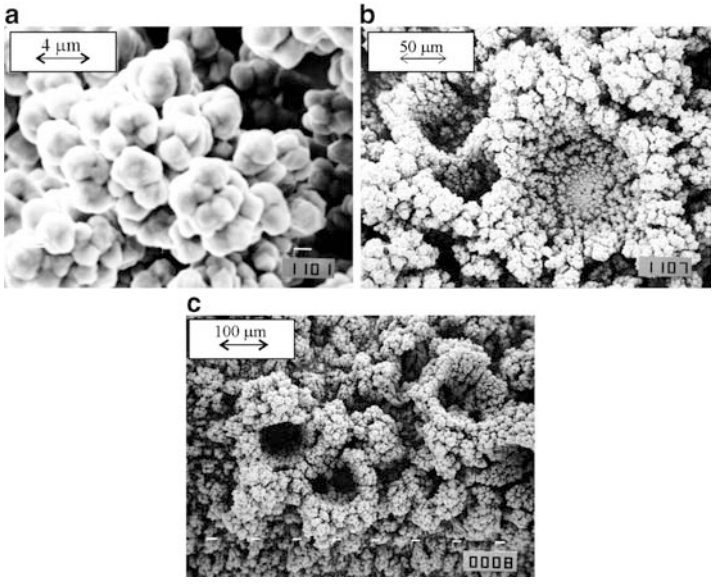

Figure 9. Copper deposit obtained at an overpotential of 800 mV. (**a**, **b**) quantity of electricity: 5.0 mA h cm^{-2} and (**c**) quantity of electricity: 10 mA h cm^{-2}. (Reprinted from Ref. [10] with permission from Elsevier).

electricity of 5.0 mA h cm^{-2}. These enlarged differences are also the consequence of the fact that some smaller grains are consumed by the larger ones,[27] as can be deduced from Figs. 3 and 4. This is also illustrated by Fig. 5a. The increase of the quantity of the

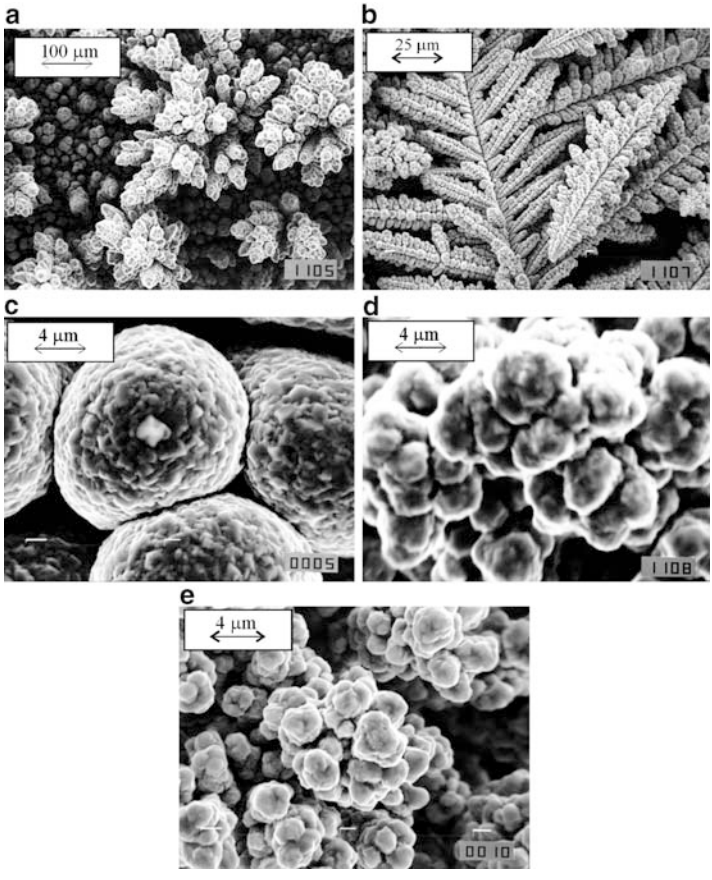

Figure 10. Copper deposits obtained with a quantity of the electricity of 20 mA h cm^{-2} and at overpotentials of: (**a**) 550 mV, (**b**) 700 mV, (**c**) 450 mV, (**d**) 800 mV, and (**e**) 1,000 mV. (Reprinted from Ref. [10] with permission from Elsevier).

electrodeposited metal led to the formation of a cauliflower-like structure (Fig. 5a, b). Furthermore, from Fig. 5a it can be seen that the spherical diffusion layers inside linear diffusion layer of the macroelectrode are formed around these cauliflower-like particles. Finally, further increase of the quantity of the electrodeposited metal produces dendritic deposit (Fig. 6).

On the other hand, it is well known that the induction time of dendrite growth initiation strongly decreases with increasing overpotential of electrodeposition.[28] The situation on the electrode surface after deposition with 2.5 mA h cm^{-2} at 700 mV (Fig. 7) is very similar to the situation after 10 mA h cm^{-2} at 550 mV (Fig. 5). The most important difference is in the shape and size of growing grains, being less globular and smaller in electrodeposition at 700 mV. Besides, the interparticle distances are relatively equal which indicate that these distances are not due to appearance of hydrogen co-deposition, which is still very small at 700 mV. Dendrites appear at 700 mV after deposition with 5.0 mA h cm^{-2} (Fig. 8).[10]

The electrodeposition at 800 mV with the quantity of the electricity of 5.0 mA h cm^{-2} (Fig. 9) did not lead to the formation of copper dendrites as at previously analyzed overpotential of 700 mV. The agglomerates of small copper grains become dominant form of the copper morphology electrodeposited at this overpotential (Fig. 9a) being similar to that from Fig. 7b. Also, there are large holes or craters between the agglomerates of these grains, which is probably due to the hydrogen co-deposition (Fig. 9b). This copper deposit is denoted as a honeycomb-like structure with craters as main characteristic,[10] as was shown earlier for copper and tin deposits in Ref. [1] The honeycomb-like structure is formed at 800 mV and with twice the quantity of electricity (Fig. 9c), as well as at an overpotential of 1,000 mV.[10] (see also Sect. III).

It is known that the hydrogen evolution effects onto the hydrodynamic conditions inside electrochemical cell.[29–31] The increase in hydrogen evolution rate leads to the decrease of the diffusion layer thickness and, hence, to the increase of limiting diffusion current density of electrode processes. It was shown[29] that if the rate of gas evolution at the electrode is larger than 100 cm^3/cm^2 min (>5 A/cm^2), the diffusion layer becomes only a few micrometers thick. It is also shown[29] that a coverage of an electrode surface with gas bubbles can be about 30%. If the thickness of the diffusion layer in conditions of natural convection is $\sim 5 \times 10^{-2}$ cm and in strongly stirred electrolyte $\sim 5 \times 10^{-3}$ cm,[32] it is clear that gas evolution is the most effective way to decrease mass transport limitations for electrochemical processes in mixed activation – diffusion control.

The overpotential η and the current density i are related by

$$\eta = \frac{b_c}{2.3} \ln \frac{i}{i_o} + \frac{b_c}{2.3} \ln \frac{1}{1 - (i/i_L)}, \tag{3}$$

where i_o, i_L, and b_c are the exchange current density, the limiting diffusion current density and cathodic Tafel slope for electrochemical process in mixed activation – diffusion control.[13] The first term in (3) corresponds to the activation part of deposition overpotential and the second one is due to the mass transfer limitations. If one and the same process takes place under two different hydrodynamic conditions, characterized by two different values of the limiting diffusion current densities $i_{L,1}$ and $i_{L,2}$, (3) can be rewritten in the forms:

$$\eta_1 = \frac{b_c}{2.3} \ln \frac{i_1}{i_o} + \frac{b_c}{2.3} \ln \frac{1}{1 - (i_1/i_{L,1})} \tag{4}$$

and

$$\eta_2 = \frac{b_c}{2.3} \ln \frac{i_2}{i_o} + \frac{b_c}{2.3} \ln \frac{1}{1 - (i_2/i_{L,2})}, \tag{5}$$

where η_1 and η_2 and i_1 and i_2 are the corresponding values of overpotentials and current densities. The same degree of diffusion control is obtained if

$$\frac{i_1}{i_{L,1}} = \frac{i_2}{i_{L,2}} \tag{6}$$

or,

$$i_2 = i_1 \frac{i_{L,2}}{i_{L,1}} \tag{7}$$

and substitution of i_2 from (7) in (5) and further rearranging gives

$$\eta_2 = \frac{b_c}{2.3} \ln \frac{i_1}{i_o} + \frac{b_c}{2.3} \ln \frac{1}{1 - (i_1/i_{L,1})} + \frac{b_c}{2.3} \ln \frac{i_{L,2}}{i_{L,1}} \tag{8}$$

and
if (4) is taken into account:

$$\eta_2 = \eta_1 + \frac{b_c}{2.3} \ln \frac{i_{L,2}}{i_{L,1}}. \tag{9}$$

Hence, if

$$i_{L,2} > i_{L,1} \tag{10}$$

in order to obtain the same degree of diffusion control in two hydrodynamic conditions, (9) must be satisfied, meaning that

$$\eta_2 > \eta_1. \tag{11}$$

The results presented here can be then explained as follows. In the absence of strong hydrogen evolution, the diffusion layer is due to the natural convection and does not depend on the overpotential of electrodeposition. As excepted, for deposition times lower than the induction time for dendritic growth initiation, the same type of deposit at larger overpotential (Fig. 7) is obtained as at lower overpotential (Fig. 5), being somewhat different in grain sizes and particle shapes.

The vigorous hydrogen evolution changes the hydrodynamic conditions and decreases the degree of diffusion control. Hence, (9) should be rewritten in the form:

$$\eta_1 = \eta_2 - \frac{b_c}{2.3} \ln \frac{i_{L,2}}{i_{L,1}}, \tag{12}$$

where η_1 becomes the effective overpotential, $\eta_1 = \eta_{eff}$, related to conditions of natural convection at which there is the same degree of diffusion control as at overpotential η_2 with the hydrogen co-deposition. Hence, the dendritic growth can be delayed or completely avoided, as can be seen from Fig. 9c, meaning that there is a really lower degree of diffusion control at an overpotential of 800 mV with the hydrogen co-deposition than at an overpotential of 700 mV where the hydrogen co-deposition is very small.

Hence, on the basis of presented results, we can propose a concept of "effective overpotential" for a metal electrodeposition. This concept is proposed – thanks to morphologies of copper deposits obtained at high deposition overpotentials (800 mV and more)[10] where the hydrogen evolution occurs. These copper deposits are probably the consequence of the stirring of electrolyte in the near-electrode layer by evolving hydrogen. This process leads to a decrease of the thickness of diffusion layer, and consequently, up to an increase of the limiting current density. According to (12), the increase of the limiting current density leads to a metal deposition at an overpotential, which is effectively lower than the specified one. Then, the obtained morphologies of copper deposits become similar to the ones obtained at some lower overpotential at which the hydrogen co-deposition does not exist.

The better understanding of the concept "effective overpotential" can be realized by taking into account the fact that the time of dendritic growth initiation depends on used deposition overpotentials. Increasing deposition overpotentials lead to decreasing times for

the beginning of dendritic growth.[28] Observing deposits obtained at overpotentials belonging to the limiting diffusion current density plateau (550 and 700 mV), one can notice that cauliflower-like forms are obtained at an overpotential of 550 mV (Fig. 5a), and dendritic forms at an overpotential of 700 mV (Fig. 8). Meanwhile, the electrodeposition with a quantity of the electricity of 20 mA h cm^{-2} leads to the formation of degenerate dendritic structure at 550 mV (Figs. 6 and 10a). Copper dendrites remain a main characteristic of the electrodeposition at 700 mV (Fig. 10b). On the other hand, it can be shown that copper dendrites are not formed by the electrodeposition at lower overpotential (for example, at 450 mV where the hydrogen evolution was also zero) with a quantity of the electricity of 20 mA h cm^{-2} (Fig. 10c). The main forms of the copper deposit obtained at this overpotential are copper globules. Also, dendritic forms are not formed with a quantity of the electricity of 20 mA h cm^{-2} and during electrodepositions at overpotentials of 800 and 1,000 mV (Fig. 10d, e). The agglomerates of copper particles remain the main characteristics of the structure of deposits obtained at these overpotentials. The macromorphology of these deposits will be discussed later.

Anyway, the structure of copper deposits obtained at overpotentials of 800 and 1,000 mV with a quantity of the electricity of 20 mA h cm^{-2} was similar to those obtained at lower overpotentials before the beginning of dendritic growth. The absence of copper dendrites at overpotentials of 800 and 1,000 mV after the electrodeposition with 20 mA h cm^{-2}, as well as the similarity of the obtained morphologies of copper deposits with those obtained at lower overpotentials before dendritic growth initiation clearly indicates that there is really lower degree of diffusion control at these overpotentials than at overpotentials of 550 and 700 mV, respectively.

The concept of "effective overpotential" can be probably applied in other cases where there is a change of hydrodynamic conditions in the near-electrode layer. The change of hydrodynamic conditions, and consequently, of metal morphologies can be caused by stirring of plating solutions in ultrasonic field,[33] in an imposed magnetic field (magnetohydrodynamic effect – MHD effect),[34–39] as well as by stirring of solution by RDE (rotating disk electrode).[40]

2. The Concept of "Effective Overpotential" Applied for Metal Electrodeposition Under an Imposed Magnetic Field

Nickel deposits obtained at a cathodic potential of −1,300 mV/SCE without and with a parallel orientation of magnetic field of 500 Oe, are shown in Fig. 11a, b, respectively. Figure 11a shows that the nickel deposit obtained without an imposed magnetic field consisted of bunch of nickel grains, while it can be seen from Fig. 11b that the nickel deposit obtained under a magnetic field with a parallel orientation to the electrode surface was a porous structure and without bunch of nickel grains.

Figure 12 shows copper deposits obtained at a cathodic potential of −500 mV/SCE without and with a magnetic field of 500 Oe applied to be parallel to the electrode surface. It can be seen from

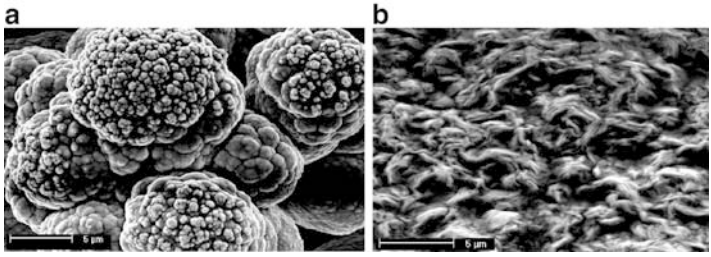

Figure 11. Nickel deposits obtained at a cathodic potential of −1,300 mV/SCE: (**a**) without and (**b**) with a magnetic field of parallel orientation of 500 Oe. (Reprinted from Ref. [39] with permission from the Serbian Chemical Society).

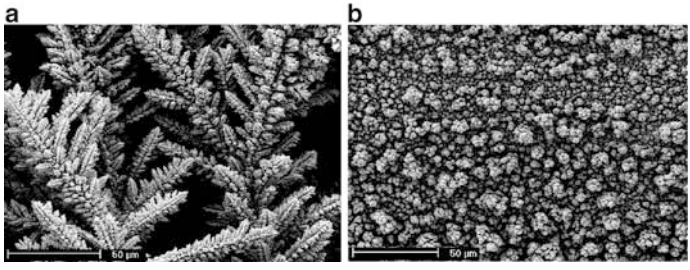

Figure 12. Copper deposits obtained at a cathodic potential of −500 mV/SCE: (**a**) without and (**b**) with a magnetic field of parallel orientation of 500 Oe. (Reprinted from Ref. [39] with permission from the Serbian Chemical Society).

this figure that the copper deposit obtained without the parallel field (Fig. 12a) had dendritic structure, while the copper deposit obtained with the parallel field (Fig. 12b) had cauliflower-like structure.

The application of the concept of "effective overpotential" for the case of the change of hydrodynamic conditions caused by magnetic field effects means that morphologies of nickel and copper deposits obtained under parallel fields (the largest magnetohydrodynamic (MHD) effect) should be, at macro level, similar to those obtained at some lower overpotentials or potentials without imposed magnetic fields. This assumption can be confirmed by the following consideration:

Figure 13a shows the nickel deposit obtained at a cathodic potential of −1,200 mV/SCE without an applied magnetic field. It can be noticed that there is similarity at a macro level between the morphology of this nickel deposit and the morphology of nickel deposit obtained at a potential of −1,300 mV/SCE under the parallel field (Fig. 11b). The both nickel deposits are without dendritic

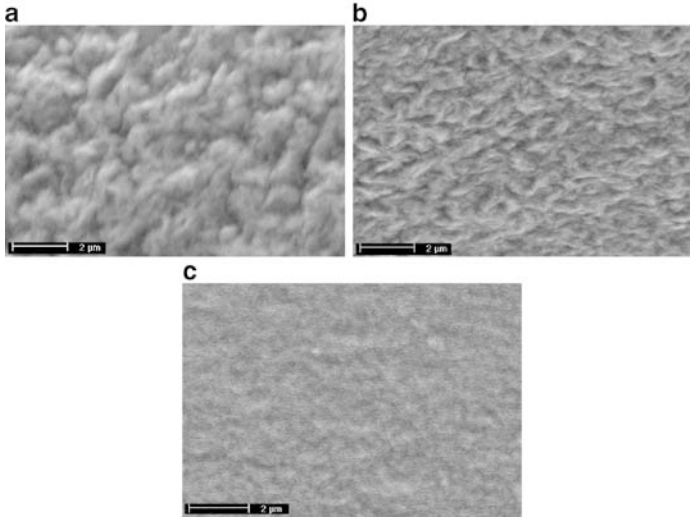

Figure 13. Nickel deposits obtained at a cathodic potential of −1,200 mV/SCE: (**a**) without, (**b**) with a magnetic field of parallel orientation of 500 Oe, and (**c**) the nickel deposit obtained at a cathodic potential of −1,000 mV/SCE without an applied magnetic field. (Reprinted from Ref. [39] with permission from the Serbian Chemical Society).

and globular parts and with clearly visible nickel grains. The only difference is in compactness of deposits, which is a consequence of larger nucleation rate and more intensive hydrogen evolution at a potential of −1,300 mV/SCE than at a potential of −1,200 mV/SCE.

Also, the concept of "effective overpotential" can be illustrated and by the comparison of the nickel deposit obtained at a cathodic potential of −1,200 mV/SCE under the parallel field with the nickel deposit obtained at −1,000 mV/SCE without an imposed magnetic field. Morphologies of these nickel deposits are shown in Fig. 13b, c. Figure 13b shows the morphology of the nickel deposit obtained at a potential of −1,200 mV/SCE under a parallel field of 500 Oe, while Fig. 13c shows the morphology of the nickel deposit obtained at −1,000 mV/SCE without an applied magnetic field. From Fig. 13b, c it can be observed that there is similarity at a macro level between these nickel deposits. The boundaries between adjacent nickel grains cannot be observed. Anyway, the nickel deposit obtained at −1,200 mV/SCE under the parallel field (Fig. 13b) was more similar to that obtained at −1,000 mV/SCE without an applied magnetic field than to that obtained at −1,200 mV/SCE without an imposed magnetic field (Fig. 13a).

This concept can be also applied for the case of the electrodeposition of copper. As mentioned earlier, the morphology of the copper deposit obtained at cathodic potential of −500 mV/SCE under the parallel field was of cauliflower-like structure (Fig. 12b), while the morphology of the copper deposit obtained without the applied magnetic field had very dendritic structure (Fig. 12a). It is known that dendritic structures are main characteristic of electrodeposition in conditions of full diffusion control, while cauliflower-like structures are a characteristic of a dominant diffusion in mixed control of electrodeposition process.[13]

Anyway, it can be seen that the application of a parallel field of 500 Oe led to shifting of the formation of characteristic morphological forms toward lower cathodic potentials for about 100–200 mV.

Of course, the influence of magnetic field appears to be restricted to the diffusion-limited regions. During electrolysis under parallel fields, the Lorentz force induces convective flow of the electrolyte close to electrode surface. A magnetically stimulated convection leads to a decrease of the diffusion layer thickness thus increasing the diffusion-limited current density.[39] As a rule, it was adopted that the limiting diffusion current density depends on magnetic field, as $i_L \propto B^{1/3}$.[41] Anyway, the increase of the

limiting current density caused by the effect of applied magnetic fields with a parallel orientation leads to a decrease of the degree of diffusion control of the deposition process, and then, the electrodeposition process occurs at some overpotential which is effectively lower. This overpotential at which a metal electrodeposition occurs when the change of hydrodynamic conditions is caused by the effect of imposed magnetic fields (i.e., by the magnetohydrodynamic effect) also represents "effective overpotential" of electrodeposition process.

Similar effects can be observed during electrodeposition in an ultrasonic field.[33] Copper deposits obtained in an ultrasonic field were compact and more ordered structure than copper deposits obtained without an effect of ultrasonic fields.

It is very clear from previous consideration that the proposed concept can be applied and for the case of electrodeposition of nickel. This concept is usable for all cases where there is the change of the hydrodynamic conditions in the near-electrode layer, which can be induced by the agitation of electrolyte by evolving hydrogen, ultrasonic and magnetic fields, or simply by vigorous stirring of an electrolyte.

III. PHENOMENOLOGY OF A FORMATION OF A HONEYCOMB-LIKE STRUCTURE DURING COPPER ELECTRODEPOSITION

The initial stage of the electrodeposition at an overpotential of 1,000 mV corresponding to the electrodeposition time of 10 s is given in Fig. 14a–d. These and other experiments whose results are presented in this section (Figs. 14–19) were performed potentiostatically from 0.15 M $CuSO_4$ in 0.50 M H_2SO_4 at a temperature of 18.0 ± 1.0°C, onto vertical stationary copper wire electrodes which were not previously covered by copper thin films. The parallelism between the process of the copper electrodeposition and the hydrogen evolution can be easily seen in Fig. 14a. From this figure, both the sites of the formation of hydrogen bubbles (i.e., sites at which the hydrogen evolution starts) and the agglomerates of copper grains between them can be noticed.

It can be seen from Fig. 14b that the hydrogen evolution reaction, as well as the copper electrodeposition are initiated at irregularities at an electrode surface. The irregularities at an electrode surface represent the most convenient sites (active centres)

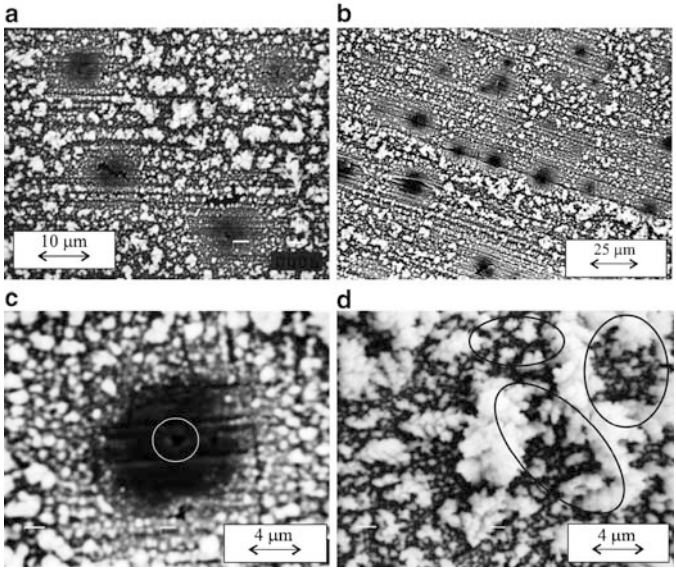

Figure 14. (**a**) Copper deposit obtained at an overpotential of 1,000 mV. Time of electrolysis: 10 s, (**b**) the positions of formation of hydrogen bubbles and agglomerates of copper grains, and (**c**, **d**) the details from Fig. 14a and b. (Reprinted from Ref. [18] with permission from Springer).

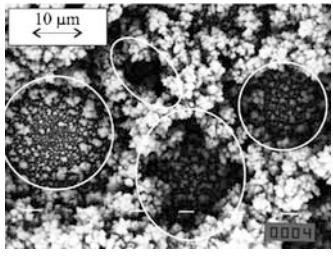

Figure 15. Copper deposit obtained at an overpotential of 1,000 mV. Time of electrolysis: 30 s. (Reprinted from Ref. [18] with permission from Springer).

for the beginning of hydrogen evolution, i.e., for the formation of hydrogen bubbles. The true position of the formation of a hydrogen bubble can be seen from Fig. 14c showing a bare part of the copper electrode (part in circle in Fig. 14c).

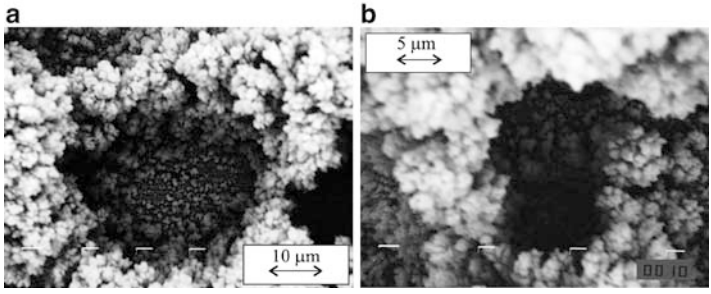

Figure 16. Copper deposit obtained at an overpotential of 1,000 mV: (**a**) "regular hole", and (**b**) "irregular hole". Time of electrolysis: 60 s. (Reprinted from Ref. [18] with permission from Springer).

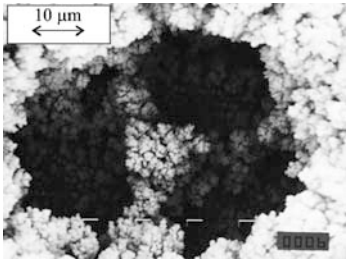

Figure 17. Copper deposit obtained at an overpotential of 1,000 mV. Time of electrolysis: 120 s. (Reprinted from Ref. [18] with permission from Springer).

The mechanism of formation of bubbles at an electrode surface has been described for a long time.[29–31,42] The gas formed at the electrode dissolves in the electrolyte, which becomes supersaturated. At the nucleation sites on the electrode, small bubbles are formed, grow to a certain size and are then detached. The higher the current density, the more the solution becomes saturated; more and more nucleation sites become active, and also the rate of growth of the bubbles increases.[31] Jenssen and Hoogland[31] also pointed out that at lower current densities, only the irregularities at the edges (formed by the cutting of the foil) are active, and the amount of bubbles formed at the lower edge is sufficient to take up all the hydrogen formed. This is no longer the case at higher current density, and then bubbles are also formed at the less deformed surface.

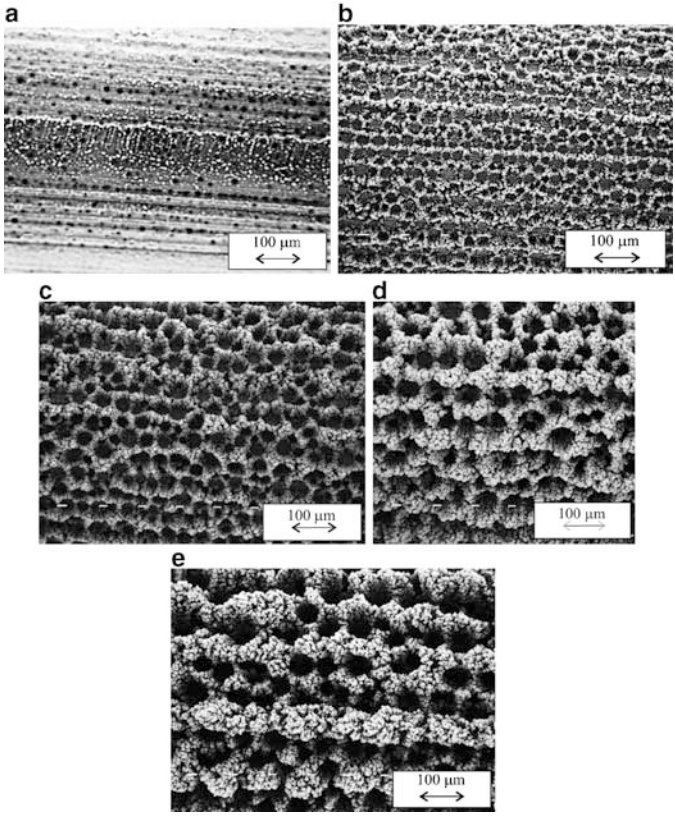

Figure 18. Copper deposits obtained at an overpotential of 1,000 mV. Time of electrolysis: (**a**) 10, (**b**) 30, (**c**) 60, (**d**) 120, and (**e**) 150 s. (Reprinted from Ref. [18] with permission from Springer).

Figure 14d shows typical agglomerates consisted of relatively small copper grains and situated between the bubbles (parts in ellipses in this figure). The different size and periodicity of agglomerates of copper grains can be explained as follows: It was assumed[43] that the active centres have different activity or different critical overpotential with respect to the formation of nuclei. The nuclei can be formed on those centres whose critical overpotential is lower or equal to the overpotential externally applied to the cell. The higher the applied overpotential, the greater the number of

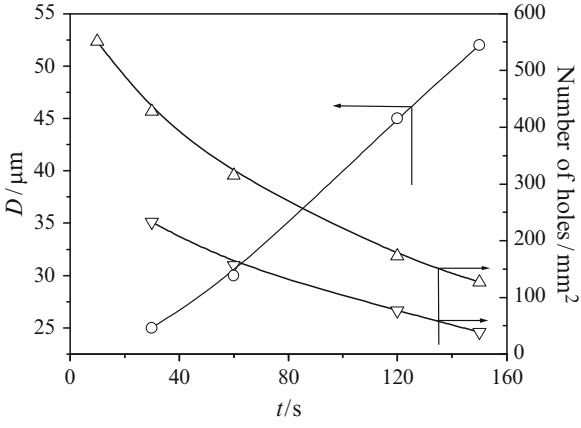

Figure 19. The dependence of average diameters of the surface holes, *D* (*open circles*), number of "regular holes" per square millimeter surface area of copper electrodes (*open triangles*) and number of "irregular holes" per square millimeter surface area of copper electrodes (*inverted traingles*) on electrolysis times. (Reprinted from Ref. [18] with permission from Springer).

active sites take part in nucleation process. The active sites are mainly placed on the irregularities at an electrode surface,[44] as can be seen in Fig. 14b. On the other hand, nucleation does not occur simultaneously over the entire cathode surface, but it is a process extended in time so that crystals generated earlier may be considerably larger in size than the ones generated later. Besides, in the case of fast electrodeposition processes, the nucleation exclusion zones around already existing nuclei are formed,[45,46] and in the case of the slower ones, there is an effect on the nucleation rate distribution around growing grains.[47,48] This causes the periodicity in the surface structure of polycrystalline electrolytic deposits.[49–51]

The copper deposit obtained with the electrodeposition time of 30 s is given in Fig. 15, from which can be seen two characteristic groups of holes or craters. The origin of one group of holes is due to the attachment of hydrogen bubbles at surface area of an electrode. These holes have regular circular shapes and, in Fig. 15 they are given in circles. The second group of holes have irregular shapes, and these holes are given in ellipses in Fig. 15. The formation of

these irregular craters is not associated with the process of hydrogen evolution, and it can be assumed that the origin of these holes is of the agglomerates of relatively small copper grains shown in Fig. 14d.

The formation of craters or holes as a consequence of the hydrogen evolution can be explained by the analysis of Figs. 14a, c and 15 in the following way: In the initial stage of the electrodeposition, hydrogen bubbles are formed at active sites at an electrode surface (Fig. 14a, b), and copper growth is blocked at these sites. These hydrogen bubbles grow with a time of electrodeposition, and in one moment, they get detached from an electrode surface realizing a fresh electrode surface for a new copper nucleation. This can be seen from Figs. 14c and 15, showing a bare copper electrode at a position where the formation of a hydrogen bubble begins (Fig. 14c) and a position of already formed hole covered with a thin copper film (parts in circles in Fig. 15). Anyway, the processes of the formation of hydrogen bubbles at active sites, their detachment from an electrode surface when critical size is reached as well as their repeated formation at growing electrode represent successive steps that led to the formation of this type of holes. The typical crater or hole formed due to the attachment of hydrogen bubbles ("regular hole"), which is obtained with the electrodeposition time of 60 s, is shown in Fig. 16a.

The explanation for the formation of the second group of craters can be given as follows: as already pointed out, at an overpotential of 1,000 mV, the process of hydrogen evolution is competitive with the process of copper electrodeposition. As a consequence of a parallel evaluation of these processes, both the sites of a formation of hydrogen bubbles and the agglomerates of copper grains between them were obtained (Fig. 14). The agglomerates of these copper grains exactly represent nucleation centres for the formation of craters or holes belonging to the other group (parts in ellipses in Fig. 14d). The further electrolysis process leads to copper nucleation and growth primarily at these agglomerates owing to the concentration of current lines at them, which will lead to a joining closely formed agglomerates and a formation of hole in one moment. This effect of current distribution at growing surface will be enhanced by the additional physical blocking of copper growth by the hydrogen bubbles preventing nucleation processes at lateral sides of the agglomerates and enhancing the nucleation processes at the top of the agglomerates. In addition, these agglomerates initiate walls, which will limit the growth of hydrogen bubbles. Hence, as a result of all these parallel

processes, holes of "irregular" shapes are formed. These holes are situated among those formed due to the attachment of hydrogen bubbles, and these craters are deeper than those obtained due to the attachment of hydrogen bubbles. The typical "irregular hole" is given in Fig. 16b, presenting a hole obtained with the electrodeposition time of 60 s.

Mechanisms describing the formation of holes of this type are based on the amplification of electrode surface coarseness[52,53] in diffusion-controlled electrodeposition and to the tip[54] and edge[55] effects of current density distribution at electrode surface. More about these mechanisms can be found in Ref. [13]

With the evaluating electrodeposition process, a coalescence of closely formed hydrogen bubbles was observed. The typical coalesced hydrogen bubble obtained at an overpotential of 1,000 mV with electrolysis time of 120 s is shown in Fig. 17. The number of holes formed of coalesced hydrogen bubbles increases with time of electrolysis. In Fig. 17, it can be seen that a structure of hole formed of coalesced hydrogen bubbles consisted of smaller holes which were mutually separated by a "bridge" of copper agglomerates. Agglomerates of copper grains that separate smaller holes inside a large hole are at a lower level than the agglomerates of copper grains around a large hole.

The decrease in a number of formed holes can be easily observed in Fig. 18, showing morphologies of copper deposits obtained with times of electrolysis of 10, 30, 60, 120, and 150 s. This decrease can be primarily ascribed to a coalescence of a closely formed hydrogen bubbles. On the other hand, the number of craters formed of an initially formed copper agglomerates also decreases with electrolysis times, and it can be expected that these craters will completely disappear with a longer time of electrolysis. This is due to the current distribution at a copper growing surface; that is, the fact that a new copper nucleation and growth primarily takes place at the edges of these holes, which will lead to totally closing and losing of holes from this group with longer electrolysis times. In this way, only the holes formed due to the hydrogen evolution will remain at a surface area of electrode.

Figure 19 shows the dependence of average diameters of craters or holes, D, formed due to the attachment of hydrogen bubbles on electrolysis time, from which the increase in average diameters of holes with the electrolysis time can be clearly seen. The dependences of the number of craters or holes formed due to the attachment

of hydrogen bubbles per square millimeter surface area ("regular holes") and those formed due to the effect of current distribution ("irregular holes") on the electrolysis time are also shown in Fig. 19. The decrease in the number of both groups of craters or holes can be observed in this figure.

The logarithm of the number of "regular holes" per square millimeter surface area of copper electrode as a function of electrolysis time gives the straight line, which points out that the decrease in number of holes with electrolysis time follows the first-order reaction low.[18] This can be very useful in the determination of the mechanism of the formation and growth of holes during metal electrodeposition in the presence of hydrogen evolution, as well as in the investigation of the different parameters that affects the honeycomb-like copper structure formation.

IV. THE EFFECT OF DEPOSITION CONDITIONS ON COPPER DEPOSITS MORPHOLOGY

1. The Surface Preparation

The initial stage of electrodeposition of copper from 0.15 M $CuSO_4$ in 0.50 M H_2SO_4 at an overpotential of 1,000 mV, onto stationary vertical copper wire electrodes previously covered by thin copper films is shown in Fig. 20. The detailed description of the formation of this type of cylindrical copper electrodes is described in Refs. [56,57] In this case, for the difference of that observed in Fig. 14b, irregularites or active centres at an electrode surface were "killed" by the electrodeposition of uniform thin copper film at an overpotential of 300 mV during 2 min.[17] Then, a higher energy was needed for the formation of hydrogen bubbles. From Fig. 20, it can be seen that a number of formed bubbles was considerably smaller than number of bubbles formed onto the electrode with active centres (Fig. 14b). Simultaneously, the diameter of the formed holes was larger, and they were random oriented at electrode surface.

Figure 21 shows copper deposits obtained at an overpotential of 1,000 mV with different quantities of the electricity, onto stationary vertical copper wire electrodes previously covered by thin copper films. The dependences of average diameters of craters or holes, D formed due to the attachment of hydrogen bubbles and number of craters or holes formed due to the attachment of hydrogen bubbles

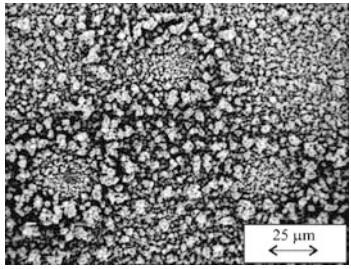

Figure 20. Copper deposit obtained at an overpotential of 1,000 mV. Time of electrolysis: 10 s. Solution: 0.15 M $CuSO_4$ in 0.50 M H_2SO_4; temperature: $18.0 \pm 1.0°C$; working electrode: copper electrode previously covered by copper thin film. (Reprinted from Ref. [18] with permission from Springer).

per square millimeter surface area ("regular holes") on electrolysis time, formed on this type of cylindrical copper electrodes are shown in Fig. 22.

Analyzing the data in Figs. 19 and 22, we can notice that average diameters of holes formed at stationary vertical copper wire electrodes which were not previously covered by copper thin films were about two times smaller than those obtained by electrodeposition onto copper electrodes previously covered with a thin copper film. On the other hand, the number of the formed holes per square millimeter surface area ("regular holes") was approximately five to ten times larger than the number of holes per square millimeter surface area obtained by electrodeposition onto copper electrodes with uniform thin copper films.

The obtained differences clearly point out the significance of preparing a working electrode for electrodeposition processes at high overpotentials, at which there is a parallelism between the process of the copper electrodeposition and the hydrogen evolution. The observed differences in average diameters of the formed holes or craters as well as in the number of the formed craters or holes can be explained as follows: the surface area of copper electrodes which were not previously covered by copper thin films consisted of a large number of irregularities, which presented active sites (centres), that is, energetic the most convenient sites for the formation

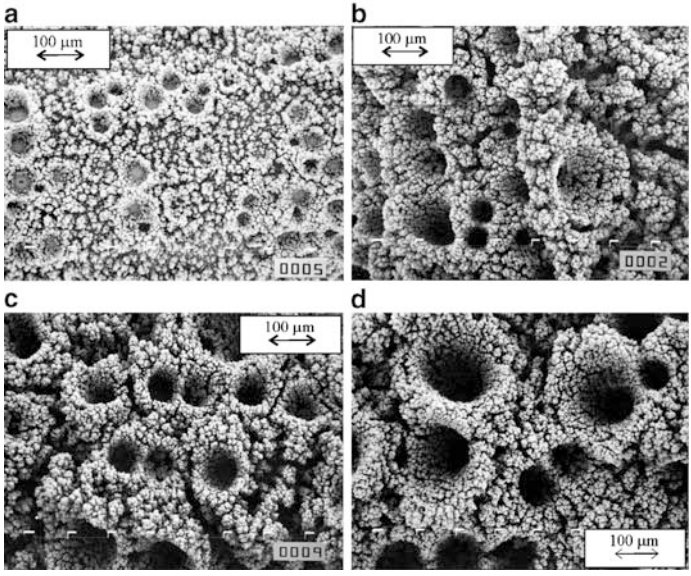

Figure 21. Copper deposits obtained potentiostatically at an overpotential of 1,000 mV. Quantities of electricity: (**a**) 2.5 mA h cm^{-2}, (**b**) 10 mA h cm^{-2}, (**c**) 15 mA h cm^{-2}, (**d**) 20 mA h cm^{-2}. Solution: 0.15 M $CuSO_4$ in 0.50 M H_2SO_4; temperature: 18.0 ± 1.0°C; working electrode: stationary vertical copper wire electrode previously covered by copper thin film. (Reprinted from Ref. [17] with permission from Elsevier).

of hydrogen bubbles. In the initial stage of electrodeposition process, the number formed hydrogen bubbles at such electrode was considerably larger than the number of bubbles formed at the electrode with "killed" active centres. Then, in the growth process, the same quantity of evolved hydrogen is distributed over larger number of hydrogen bubbles, resulting in the formation of honeycomb-like structure with larger number of holes with smaller diameters.

2. The Effect of Concentration of Cu(II) Ions

Figure 23 shows the polarization curves for the copper electrodeposition from 0.075 M $CuSO_4$ in 0.50 M H_2SO_4 (*solution (I)*), 0.30 M $CuSO_4$ in 0.50 M H_2SO_4 (*solution (II)*) and 0.60 M $CuSO_4$ in 0.50 M H_2SO_4 (*solution (III)*). All experiments whose results are presented in Figs. 23–30 and Table 1 were performed

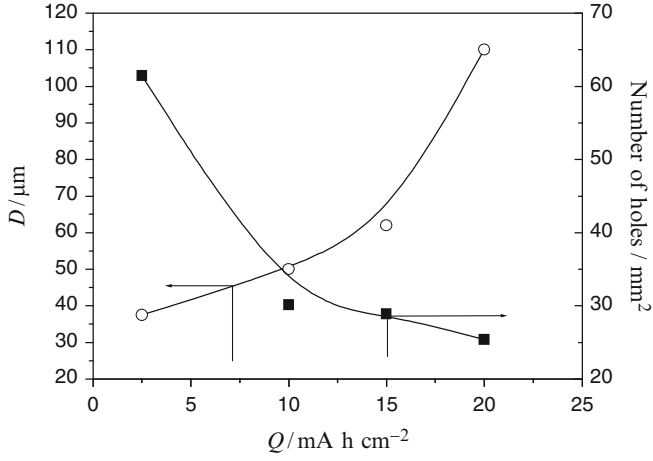

Figure 22. The dependence of average diameters of the surface holes, *D*, (*open circles*) and number of "regular holes" per square millimeter surface area of copper electrodes (*closed squares*) on the quantity of the electricity. (Reprinted from Ref. [17] with permission from Elsevier).

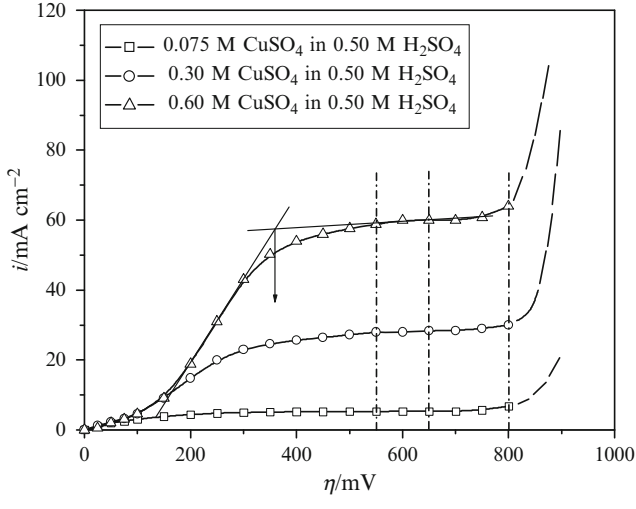

Figure 23. Polarization curves for the cathodic process of copper deposition from: 0.075 M $CuSO_4$ in 0.50 M H_2SO_4 (*solution (I)*), 0.30 M $CuSO_4$ in 0.50 M H_2SO_4 (*solution (II)*), and 0.60 M $CuSO_4$ in 0.50 M H_2SO_4 (*solution (III)*). (Reprinted from Ref. [19] with permission from MDPI).

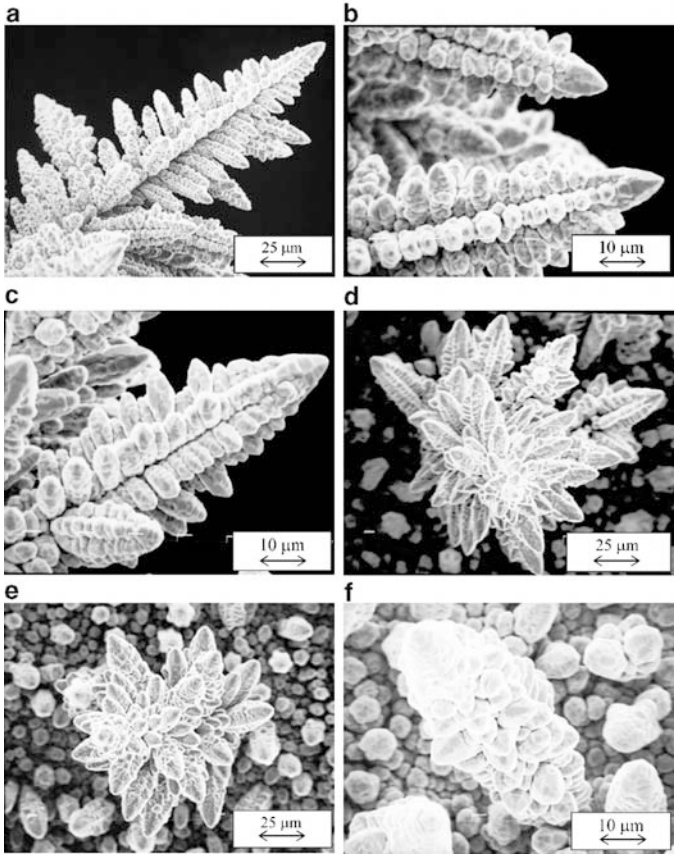

Figure 24. Copper deposits obtained at an overpotential of 650 mV. Quantity of electricity: 10 mA h cm^{-2}. (**a**, **b**): *solution (I)*; (**c**, **d**): *solution (II)*; (**e**, **f**): *solution (III)*. (Reprinted from Ref. [19] with permission from MDPI).

potentiostatically at a temperature of 18.0 ± 1.0°C. The beginning of the plateau of the limiting diffusion current density is determined as the intersect of straight lines joining currents in mixed activation – diffusion and diffusion control of electrodeposition, as shown in the Fig. 23. The end of this plateau is determined as the overpotential at which current starts to grow with the increasing overpotential. The increase in the concentration of Cu(II) ions leads

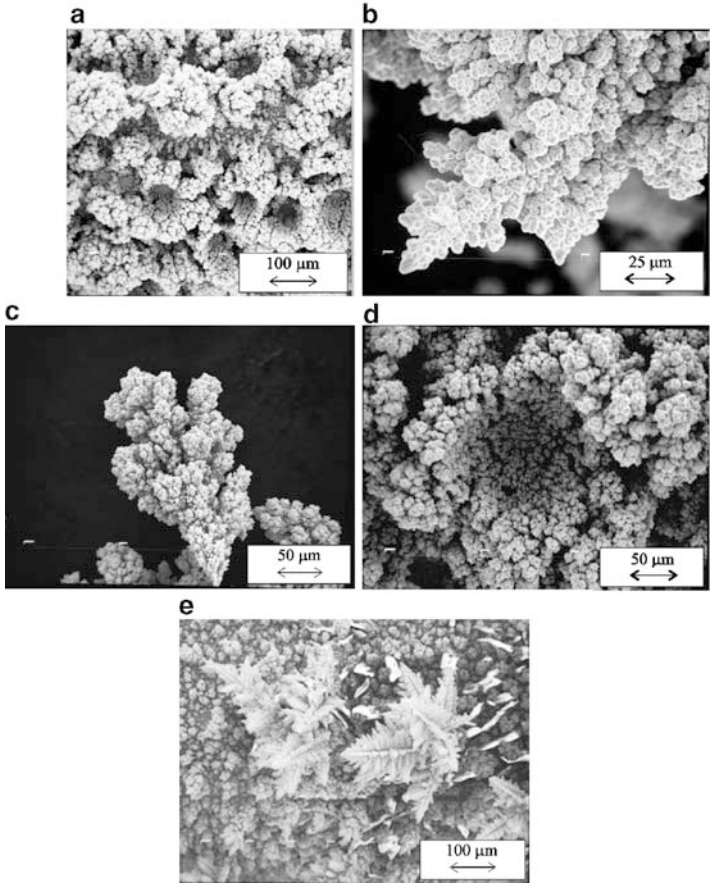

Figure 25. Copper deposits obtained at an overpotential of 800 mV. Quantity of electricity: 10 mA h cm^{-2}. (**a**) *solution (I)*; (**b**–**d**) *solution (II)*; (**e**) *solution (III)*. (Reprinted from Refs. [15, 60] with permissions from MDPI and Elsevier).

to a shift of overpotentials at which the limiting diffusion current density plateaus initiate toward the larger overpotentials, while the end of these plateaus remains practically constant (Fig. 23).

The effect of hydrogen evolution on copper electrodeposition was examined at overpotentials of 550, 650, 800, and 1,000 mV. For all examined solutions, overpotentials of 550 and 650 mV corresponded to the plateau of the limiting diffusion current density,

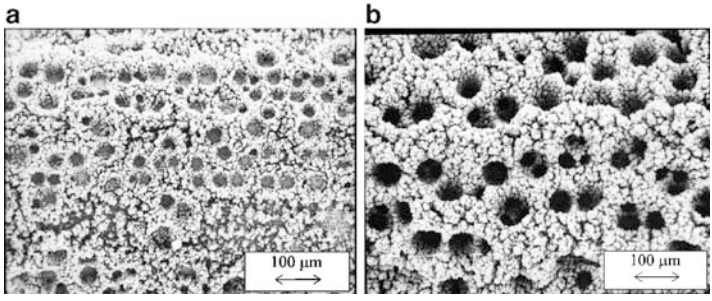

Figure 26. Copper deposits obtained at an overpotential of 1,000 mV from 0.075 M $CuSO_4$ in 0.50 M H_2SO_4. Quantity of electricity: (**a**) 2.5 mA h cm^{-2}, (**b**) 20 mA h cm^{-2}. (Reprinted from Ref. [58] with permission from Elsevier).

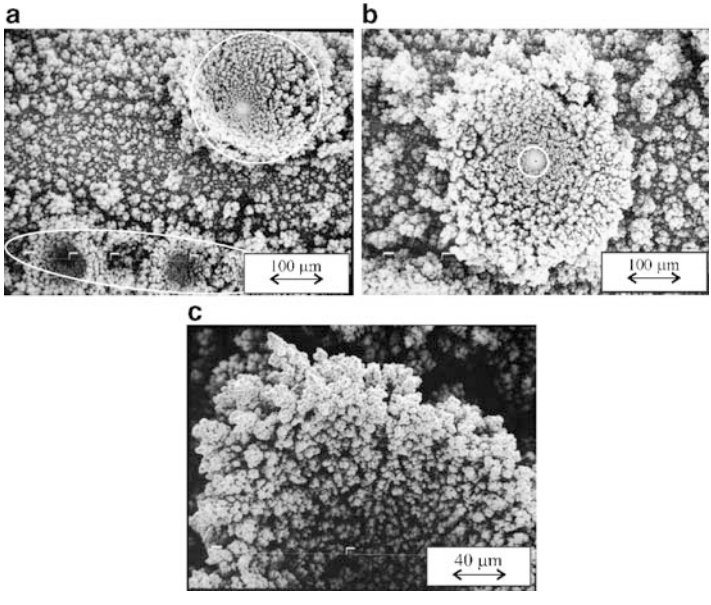

Figure 27. Copper deposits obtained at an overpotential of 1,000 mV from 0.30 M $CuSO_4$ in 0.50 M H_2SO_4. (**a**) Quantity of the electricity: 2.5 mA h cm^{-2}, (**b**, **c**) quantity of the electricity: 5.0 mA h cm^{-2}. (Reprinted from Ref. [58] with permission from Elsevier).

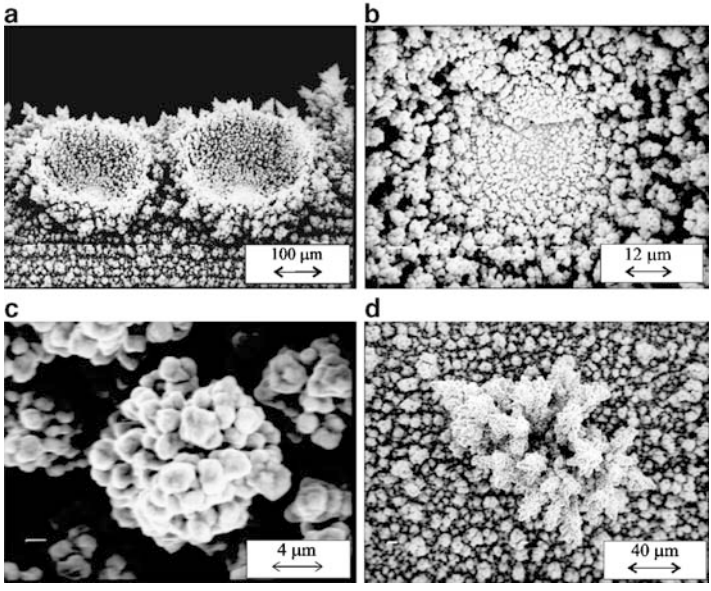

Figure 28. Copper deposits obtained at an overpotential of 1,000 mV from 0.60 M $CuSO_4$ in 0.50 M H_2SO_4: (**a**) dish-like holes, (**b**) the bottom, and (**c**) the wall of the dish-like hole, and (**d**) dendrite formed between holes. Quantity of the electricity: 2.5 mA h cm^{-2}. (Reprinted from Ref. [58] with permission from Elsevier).

while overpotentials of 800 and 1,000 mV were about 50 and 250 mV outside the plateau of the limiting diffusion current density, respectively (Fig. 23).

The summary of the obtained values of the average current efficiencies of hydrogen evolution in the dependence of concentration of Cu(II) ions and overpotential of electrodeposition[19,58] are given in Table 1.

It can be seen from Table 1 that the average current efficiencies of hydrogen evolution, $\eta_{av}(H_2)$ decreased with the increasing $CuSO_4$ concentration at all overpotentials. At the first sight, this was unexpected because the concentration of H_2SO_4 was same for all solutions. The explanation for it can be obtained by the analysis of ionic equilibrium of the species in the $CuSO_4$–H_2SO_4–H_2O system (Fig. 1). According to this equilibrium, it is the result of decreasing the hydrogen ion concentration with the increasing copper concentration.[59]

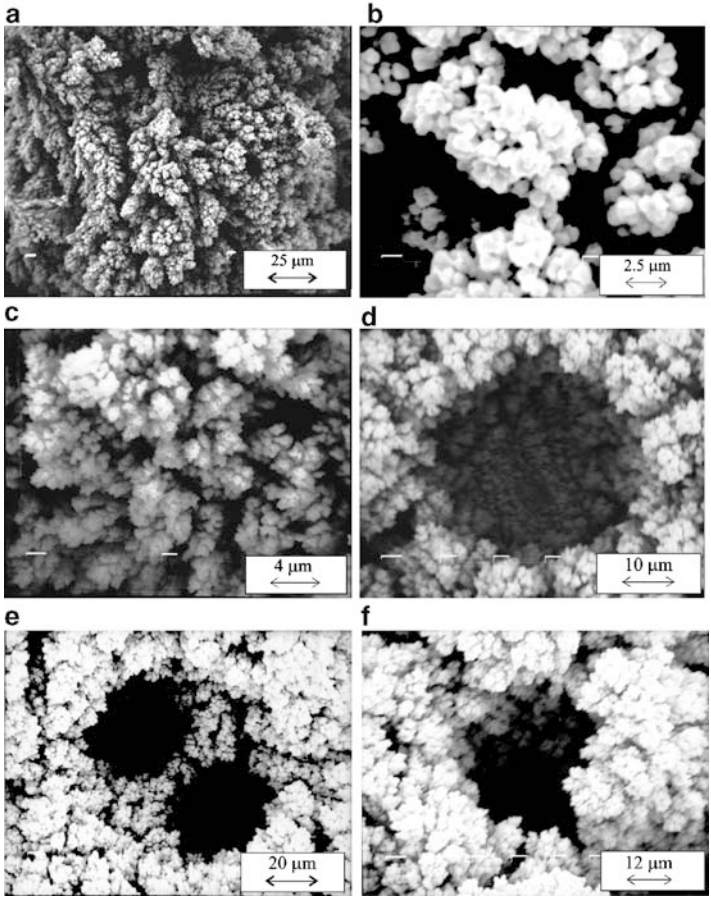

Figure 29. Copper deposits obtained at an overpotential of 1,000 mV from 0.075 M $CuSO_4$ in 0.50 M H_2SO_4: (**a, b, e, f**) quantity of the electricity: 20 mA h cm^{-2}, (**c, d**) quantity of the electricity: 5.0 mA h cm^{-2}. (Reprinted from Ref. [58] with permission from Elsevier).

(i) Morphologies of Copper Deposits Obtained at Overpotentials up to 800 mV

The copper deposit electrodeposited from 0.075 M $CuSO_4$ in 0.50 M H_2SO_4 at an overpotential of 550 mV with a quantity of the electricity of 10 mA h cm^{-2} was cauliflower-like structure. Copper

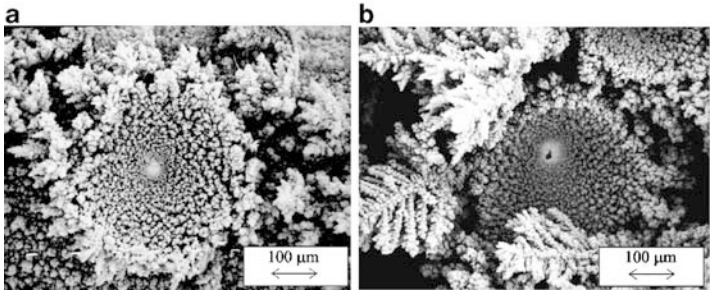

Figure 30. Copper deposits obtained at an overpotential of 1,000 mV from 0.60 M $CuSO_4$ in 0.50 M H_2SO_4: (**a**) quantity of the electricity: 5.0 mA h cm^{-2}, (**b**) quantity of the electricity: 20 mA h cm^{-2}. (Reprinted from Ref. [58] with permission from Elsevier).

Table 1.
The average current efficiencies of hydrogen evolution in the function of concentration of Cu(II) ions. (Reprinted from Refs. [19,58] with permissions from MDPI and Elsevier).

	The average current efficiencies of hydrogen evolution, $\eta_{av}(H_2)$ (in %), at overpotentials of:		
Solution for copper Electrodeposition	650 mV	800 mV	1,000 mV
0.075 M $CuSO_4$ in 0.50 M H_2SO_4	7.5	42.2	68.7
0.30 M $CuSO_4$ in 0.50 M H_2SO_4	0.83	3.5	16.0
0.60 M $CuSO_4$ in 0.50 M H_2SO_4	0	0.66	4.6

deposits electrodeposited from 0.30 M and 0.60 M $CuSO_4$ in 0.50 M H_2SO_4 at the same overpotential and with the same quantity of the electricity were globular structures.[19] Electrodepositions of copper with two times larger than the quantity of electricity led to the change of morphology of copper deposits. Copper dendrites were formed during electrodeposition of copper from *solution (I)*, while the mixture of cauliflower-like and globular forms was obtained by electrodeposition from *solution (II)* and *solution (III)*. At this overpotential, there was hydrogen evolution only from *solution (I)* (the average current efficiency of hydrogen evolution, $\eta_{av}(H_2)$, was 1.7%).[19]

Morphologies of copper deposits obtained at an overpotential of 650 mV from 0.075 M, 0.30 M, and 0.60 M $CuSO_4$ in 0.50 M H_2SO_4

are shown in Fig. 24. It can be seen from Fig. 24 that copper dendrites were formed during copper electrodeposition from all three solutions. Meanwhile, it is very clear from Fig. 24 that the shape of copper dendrites depended strongly on the concentration of Cu(II) ions. Very branchy copper dendrites consisting of corncob-like elements were formed from *solution (I)* (Fig. 24a, b). Copper dendrites formed from *solution (II)* presented a mixture of very branchy dendritic forms (Fig. 24c) and those shaped like flowers (Fig. 24d). Finally, the copper deposits obtained from *solution (III)* presented a mixture of flower-like (Fig. 24e) and corncob-like forms (Fig. 24f).

Figure 25 shows the morphologies of copper deposits obtained at an overpotential of 800 mV, from which the strong effect of concentration of Cu(II) ions on copper electrodeposition can be seen.

The honeycomb-like structure was formed from *solution (I)* (Fig. 25a).

A mixture of dendritic forms (Fig. 25b), degenerate dendrites (Fig. 25c), and holes formed due to the attached hydrogen bubbles (Fig. 25d) was obtained by electrodeposition from *solution (II)*.

Finally, only dendritic copper forms are obtained from *solution (III)* (Fig. 25e). These dendritic forms were more branchy structures than those formed from the same solution by the electrodeposition at an overpotential of 650 mV and with the same quantity of the electricity (cf. Fig. 24e, f).

The careful analysis of the morphologies of copper deposits shown in Figs. 24 and 25 indicated that an increase in the concentration of Cu(II) ions led to a shift of the formation of characteristic morphological shapes of copper deposits toward higher electrodeposition overpotentials by about 100–150 mV. This is because of the increase of a critical overpotential of dendritic growth initiation with the increase of concentration of Cu(II) ions.[19] For example, copper dendrites formed at 800 mV from *solution (III)* (Fig. 25e) were very similar to those obtained at 650 mV from *solutions (I)* and *(II)* (Fig. 24a–c). The globular forms obtained from *solutions (II)* and *(III)* at an overpotential of 550 mV were very similar to ones obtained from 0.15 M $CuSO_4$ in 0.50 M H_2SO_4 at an overpotential of 450 mV.[10] The different shapes of copper dendrites formed at an overpotential of 650 mV from solutions with different concentrations of Cu(II) ions (Fig. 24) also pointed out the strong effect of concentration of Cu(II) ions on electrodeposition of copper at an overpotential of 650 mV.

(ii) Morphologies of Copper Deposits Obtained at an Overpotential of 1,000 mV

The copper deposits obtained from 0.075 M $CuSO_4$ in 0.50 M H_2SO_4 at an overpotential of 1,000 mV with the quantities of electricity of 2.5 and 20 mA h cm^{-2} are shown in Fig. 26, from which it can be seen that honeycomb-like structures were formed by electrodepositions from this solution.

The copper deposits obtained at an overpotential of 1,000 mV from 0.30 M $CuSO_4$ in 0.50 M H_2SO_4 with quantities of electricity of 2.5 and 5.0 mA h cm^{-2} are shown in Fig. 27, from which it can be clearly seen that the structures of the deposits obtained from 0.30 M $CuSO_4$ in 0.50 M H_2SO_4 were completely different from those obtained from 0.075 M $CuSO_4$ in 0.50 M H_2SO_4 (Fig. 26).

Two types of craters or holes formed due to the attachment of hydrogen bubbles can be observed by analysis of the copper deposit shown in Fig. 27a. One type of holes is presented in the ellipse in Fig. 27a. These holes are similar to those forming the honeycomb-like structure during copper electrodeposition from 0.075 M $CuSO_4$ in 0.50 M H_2SO_4. These holes are grouped and mutually separated by agglomerates of relatively small copper grains.

The other type of holes is shown in the circle in the same figure. From Fig. 27a, it can be seen that the shape of this hole is dish or shell-like. The diameter of dish-like holes is larger than the diameter of the holes forming the honeycomb-like structure, while their number is smaller than the number of holes forming the honeycomb-like structure. A typical dish-like hole electrodeposited with the quantity of the electricity of 5.0 mA h cm^{-2} is shown in Fig. 27b. The bottom of the dish-like hole is covered by almost compact copper deposit (the part in the circle in Fig. 27b), while the wall of this hole consists of small, very disperse agglomerates of copper grains (Fig. 27c). From Fig. 27c, it can also be seen that copper dendrites were formed at the shoulders of the dish-like holes electrodeposited with this quantity of electricity. Also, cauliflower-like forms were formed between the holes or craters belonging to these different types (Fig. 27a).

The electrodeposition processes at an overpotential of 1,000 mV from 0.60 M $CuSO_4$ in 0.50 M H_2SO_4 led to the formation of dish-like holes only. The typical dish-like holes formed with the quantity of the electricity of 2.5 mA h cm^{-2} are shown in Fig. 28a, from which it can be seen that copper dendrites were formed at their

shoulders. The bottom of the dish-like holes was almost compact (Fig. 28b), while the interior of the hole was constructed of disperse agglomerates of copper grains (Fig. 28c). Very branched copper dendrites and small cauliflower-like forms were formed among the dish-like holes during the electrodeposition of copper from this solution (Fig. 28d).

On the basis of the presented analysis of the electrodeposition processes at an overpotential of 1,000 mV (Figs. 26–28), it is obvious that increasing the concentration of Cu(II) ions leads to a change in the shape of the holes from those forming a honeycomb-like structure to dish-like holes.

It should be noted that the honeycomb-like structure was formed from 0.075 M $CuSO_4$ in 0.50 M H_2SO_4 at an overpotential of 1,000 mV, with a considerably larger quantity of co-deposited hydrogen ($\eta_{av}(H_2) = 68.7\%$) than that formed by electrodeposition at 800 mV from the same solution ($\eta_{av}(H_2) = 42.2\%$),[19]) or from 0.15 M $CuSO_4$ in 0.50 M H_2SO_4 at 800 mV ($\eta_{av}(H_2) = 10.8\%$) and 1,000 mV ($\eta_{av}(H_2) = 30.0\%$).[10] It was found[19,58] that the maximum $CuSO_4$ concentration (in 0.50 M H_2SO_4) which enabled the formation of the honeycomb-like structure was 0.15 M. The critical quantity of evolved hydrogen leading to the change of the hydrodynamic conditions in the near-electrode layer for this solution group was estimated to correspond to $\eta_{av}(H_2)$ of 10.0%.[19]

The more vigorous hydrogen evolution at this overpotential from 0.075 M $CuSO_4$ in 0.50 M H_2SO_4 makes a more visible channel structure formed through the interior of the deposit. A typical channel structure is shown in Fig. 29a, which was obtained by manipulation of the copper deposit in order that the cross section view could be seen. The top view of a part of the copper deposit shown in Fig. 29a is shown in Fig. 29b, from which it can be seen that irregular channels are distributed over the surface area of the deposit among disperse agglomerates of copper grains. These channels were generated in situ by the simultaneous processes of copper growth and vigorous hydrogen evolution. It is also known[61] that a channel or a stream copper structure can be formed ex situ by the use of an acoustically excited Ar gas bubble.

Naturally, both the formation holes and channels through the interior of the deposit occur simultaneously, and these processes can not be observed separately. As already stated, in the initial stage of the electrodeposition process, both nuclei of copper and "nuclei"

of hydrogen bubbles are formed at the active sites of the electrode surface.[18] The hydrogen bubbles isolate the substrate and then the current lines are concentrated around these hydrogen bubbles making rings consisted of agglomerates of copper grains around them. The current lines are also concentrated at the nuclei of copper formed in the initial stage between the hydrogen bubbles. Anyway, the bubbles cause an increase of the local current density around them, resulting in a faster growth of the copper deposit around the growing bubbles, as well as in increasing rate of hydrogen evolution.

As a result of the current distribution at the growing copper surface, new copper nucleation and hydrogen evolution will occur primarily at the top of these agglomerates. Some of the new, small, freshly formed hydrogen bubbles which are formed at agglomerates around previously formed large hydrogen bubbles will coalesce with them, leading to their growth with electrolysis time as already shown.[18] This is confirmed by the very porous structure of the interior of walls of the holes (Fig. 29c), which consist of disperse agglomerates of copper grains among which numerous irregular channels are present. A typical hole formed of growing hydrogen bubbles is shown in Fig. 29d. In the growth process, the coalescence of closely formed large hydrogen bubbles can also be observed (Fig. 29e).

Meanwhile, some of the freshly formed hydrogen bubbles will not find a way to coalesce with the large hydrogen bubbles because they are situated among copper nuclei which initiate a barrier for their development into large hydrogen bubbles. This effect, with already discussed current density distribution will lead to the formation of a porous channel structure through the interior of the copper deposit (Fig. 29a).

Simultaneously, holes of irregular shapes (Fig. 29f) were formed from nuclei of copper formed in the initial stage of the electrodeposition between the hydrogen bubbles.[18] The current distribution at the growing copper surface was responsible for the formation of this type of hole.

Anyway, there are two effects of hydrogen evolution on copper electrodeposition leading to the formation of the honeycomb-like structures. The first effect is a stirring of the solution in the near-electrode layer caused by a vigorous hydrogen evolution leading to the decrease of the diffusion layer thickness and the increase of the limiting diffusion current density.[10] The second effect concerns

the morphology of the copper deposits due to the effect of hydrogen bubbles on the current density distribution on the growing electrode surface. The uniform distribution of morphological forms on the electrode surface means the same hydrodynamic conditions exist over the whole electrode surface and the honeycomb-like structure indicates to the local effect of hydrogen bubbles.

Dish-like holes were formed from the more concentrated solution (0.60 M $CuSO_4$ in 0.50 M H_2SO_4), accompanied by a considerably lower quantity of evolved hydrogen ($\eta_{av}(H_2) = 4.6\%$) than was the case with the holes forming a honeycomb-like structure (0.075 M and 0.15 M $CuSO_4$ in 0.50 M H_2SO_4).

On the basis of the obtained value of the average current efficiency of hydrogen evolution of 4.6% and morphologies of copper deposits shown in Fig. 28 (very branchy copper dendrites developed between dish-like craters or holes), it is clear that the hydrogen evolution was insufficient to produce effective stirring of the solution in the near-electrode layer, which would lead to a decrease of the diffusion layer thickness, and consequently, no change in the hydrodynamic conditions and no inhibition of dendritic growth. The electrodeposition process was primarily controlled by the diffusion of ions to the electrode surface, rather than the kinetics of the electrodeposition.[13,23]

The initial stage of the formation of dish-like holes was the same as the initial stage of the formation of the honeycomb-like structure. The nuclei of copper and the "nuclei" of hydrogen bubbles were formed at active sites on the electrode surface and the formed hydrogen bubbles isolate the substrate causing a concentration of the current lines around them. Meanwhile, because of the low hydrogen co-deposition current density, the number of the formed "nuclei" of hydrogen bubbles was smaller than the number which led to the formation of the honeycomb-like structure. In the growth process, they have enough space to develop into large bubbles, making holes with a dish-like shape at the surface area of electrode. Dendrites formed at their shoulders (Fig. 28a) as well as very developed dendrites between them (Fig. 28d) clearly indicate the insufficiency of the evolved hydrogen to disturb the diffusion layer of the macroelectrode. Further copper nucleation and hydrogen evolution primarily occur at the shoulders of the growing holes and the copper dendrites between them. Most of the freshly formed hydrogen bubbles at the shoulder of the dish-like holes coalesce with

previously formed large hydrogen bubbles, leading to their growth with the electrolysis time (Fig. 30a) and making the interior of holes very porous and constructed of cauliflower- or raspberry-like forms. At the same time, the almost compact deposit at the bottom of the dish-like holes represents the position of the formation of the initial bubble (Fig. 28b), and it can be supposed that its origin is the thin copper film previously electrodeposited at 400 mV. It is of interest to note that regardless of the quantity of electricity passed, or the deposition time, the dendrites grew only at the edges of the dish-like holes. This is due to the fact that the electrodeposition of copper occurs on the dendrite branches in the same way as on any other part of the electrode surface, except on the tip of the dendrite protrusions themselves, where the process is under activation control, resulting in regular dendritic forms (Fig. 30b).[62–64] At larger deposition times, the growth of dendrites become dominant and the dish-like protrusion cease to grow. Also, it can be seen from Figs. 28a and 30a that in the "shadow" of the dish-like holes there is a lower density of grains on the initial substrate relative to the overshadowed parts of electrode, which is the consequence of the concentration of current lines at them.

In dependence on the quantity of electricity, the average diameter of the dish-like holes was in the range of 200–360 μm. The number of dish-like holes was estimated to be 2.5 holes/mm^2 surface area of the copper electrode, and it did not change with the quantity of the electricity, which can be explained by the absence of coalescence of the formed hydrogen bubbles. The comparative dependences of the average diameters, D, and the number of holes per square millimeter surface area of copper electrodes on the quantity of the electricity for both, dish-like holes and holes making the honeycomb-like structure during the electrodeposition at 1,000 mV from 0.075 M $CuSO_4$ in 0.50 M H_2SO_4 are shown in Fig. 31, from which it can be seen that the number of formed dish-like holes per square millimeter surface area of the copper electrode was considerably smaller than the number of holes forming the honeycomb-like structure and that the average diameter of the dish-like holes was about five times larger than the average diameter of the holes forming the honeycomb-like structure. This illustrates successfully the fact that a smaller number of "nuclei" of hydrogen bubbles is formed in the initial stage of electrodeposition of dish-like holes in relation to the number of formed "nuclei" of hydrogen bubbles leading to the formation of the honeycomb-like structure.

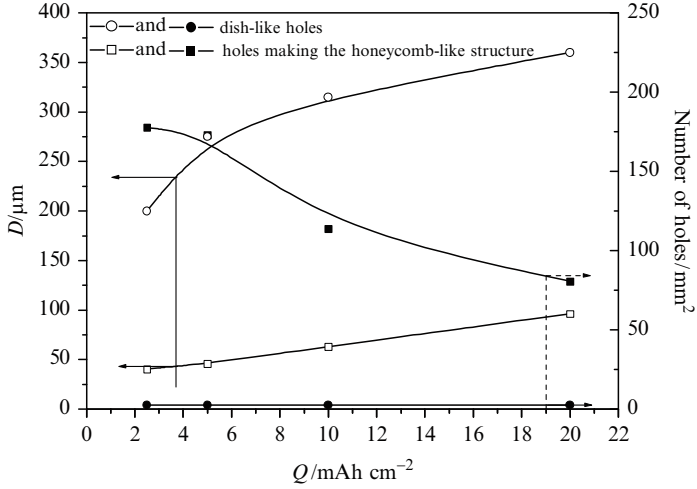

Figure 31. The dependence of average diameters of the surface holes, *D*, (*open style*) and number of holes per square millimeter surface area of copper electrodes (*solid style*) on quantities of electricity, for electrodepositions of copper from 0.075 M $CuSO_4$ in 0.50 M H_2SO_4 and 0.60 M $CuSO_4$ in 0.50 M H_2SO_4. (Reprinted from Ref. [58] with permission from Elsevier).

Furthermore, the morphology of the copper deposit obtained from 0.60 M $CuSO_4$ in 0.50 M H_2SO_4 at an overpotential of 1,000 mV consisted of all the morphological forms characteristic for copper electrodeposition at high overpotentials: holes formed due to hydrogen evolution (Fig. 28a), dendritic forms (Fig. 28d), and small cauliflower-like forms (Fig. 28d). The formation of these different morphological forms which leads to nonuniformity of the electrode surface can be explained by different local electrodeposition conditions inside the diffusion layer of the macroelectrode. It is known[65] that electrochemical processes on microelectrodes in bulk solution can be under activation control at overpotentials which correspond to the plateau of the limiting diffusion current density of the macroelectrode. Bockris et al.[63,64] and Popov et al.[62] showed that electrodeposition to the tip of a dendrite, consequently to a microelectrode, inside the diffusion layer of the macroelectrode is under activation control, while the same process is simultaneously under full diffusion control on the macroelectrode. In the absence of dendrite precursors, some cauliflower-like forms can be formed

on the surface of the macroelectrode when the electrodeposition process is under full linear diffusion control. Then, local spherical diffusion layers inside the diffusion layer of the macroelectrode are formed around them.[10] Hence, for defined electrodeposition conditions, control of the electrodeposition process at some specified points of the macroelectrode can be different from the process control at the macroelectrode in general. This explains and the nonuniformity of the electrode surface obtained from 0.60 M $CuSO_4$ in 0.50 M H_2SO_4.

The polarization characteristic of a macroelectrode is easy to determine, as well as the kind of mass transfer control on it. It is very difficult, or even impossible, to do the same for some specified points on it. On the other hand,[13,66] the morphology of metal deposits indicates the conditions under which they were formed. Hence, from the local morphology of a deposit, the type of process control on selected points of the macroelectrode can be derived.

The morphology of the copper deposit obtained at an overpotential of 1,000 mV from 0.30 M $CuSO_4$ in 0.50 M H_2SO_4 presented a mixture of morphological forms characteristic for copper deposits obtained from solutions with lower (0.075 M) and higher (0.60 M) concentrations of Cu(II) ions. Thus, a mixture of both types of holes was obtained by the electrodeposition at this overpotential from 0.30 M $CuSO_4$ in 0.50 M H_2SO_4. It was estimated that the percent of holes forming the honeycomb-like structure was about 80% of the total number of formed holes. On the basis of this fact, it can be concluded that for a concentration of supporting electrolyte of 0.50 M H_2SO_4, the concentration of 0.30 M $CuSO_4$ presents the transitional concentration between lower and higher concentrations of Cu(II) ions. This could be explained by different hydrodynamic conditions at different points of the electrode surface.

3. The Effect of Concentration of H_2SO_4

The polarization curves for the electrodeposition of copper from 0.15 M $CuSO_4$ with the addition of 0.125, 0.25, and 1.0 M H_2SO_4 are shown in Fig. 32. All experiments whose results are presented in Figs. 32–37 and Table 2 were performed potentiostatically at a temperature of 18.0 $\pm$ 1.0°C. It can be seen from Fig. 32 that the beginning of the plateau of the limiting diffusion current density was slightly shifted to higher electrodeposition overpotentials with the decreasing concentration of H_2SO_4. The ends of the plateau of

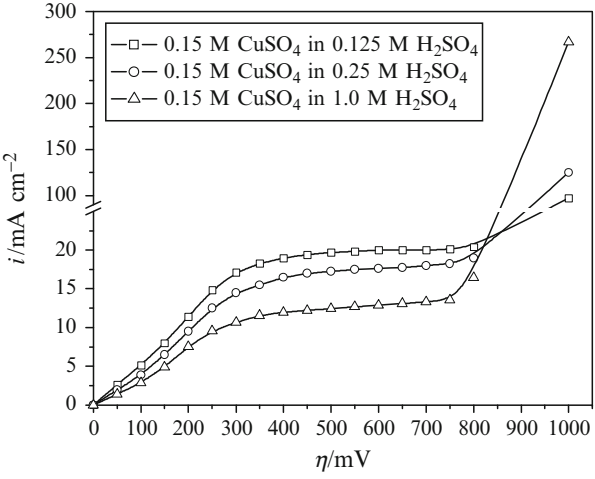

Figure 32. Polarization curves for the cathodic process of copper deposition from: 0.15 M $CuSO_4$ in 0.125 M H_2SO_4, 0.15 M $CuSO_4$ in 0.25 M H_2SO_4, and 0.15 M $CuSO_4$ in 1.0 M H_2SO_4. (Reprinted from Ref. [67] with permission from Elsevier).

the limiting diffusion current density practically do not depend on the concentration of H_2SO_4 and they correspond to an overpotential of about 750 mV. The negligible shifting of the end of the plateau of the limiting diffusion current density to lower electrodeposition overpotentials can be only observed at a polarization curve obtained from 0.15 M $CuSO_4$ in 1.0 M H_2SO_4. At overpotentials higher than 750 mV, the fastest growth of current with increasing overpotential is obtained from 0.15 M $CuSO_4$ in 1.0 M H_2SO_4 and it decreases with the decrease of the H_2SO_4 concentration. The limiting diffusion current density value decreased with the increasing concentration of H_2SO_4. The decrease in the values of the limiting diffusion current density with increasing H_2SO_4 concentration is a consequence of the decrease of the Cu(II) ion activity with increasing acidity of the solution.

The effect of hydrogen evolution on copper electrodeposition was examined at overpotentials of 550, 650, 800, and 1,000 mV. At an overpotential of 550 mV, there was hydrogen evolution only from 0.15 M $CuSO_4$ in 1.0 M H_2SO_4 (the average current efficiency of hydrogen evolution, $\eta_{av}(H_2)$, was 0.75%).[67] The summary of

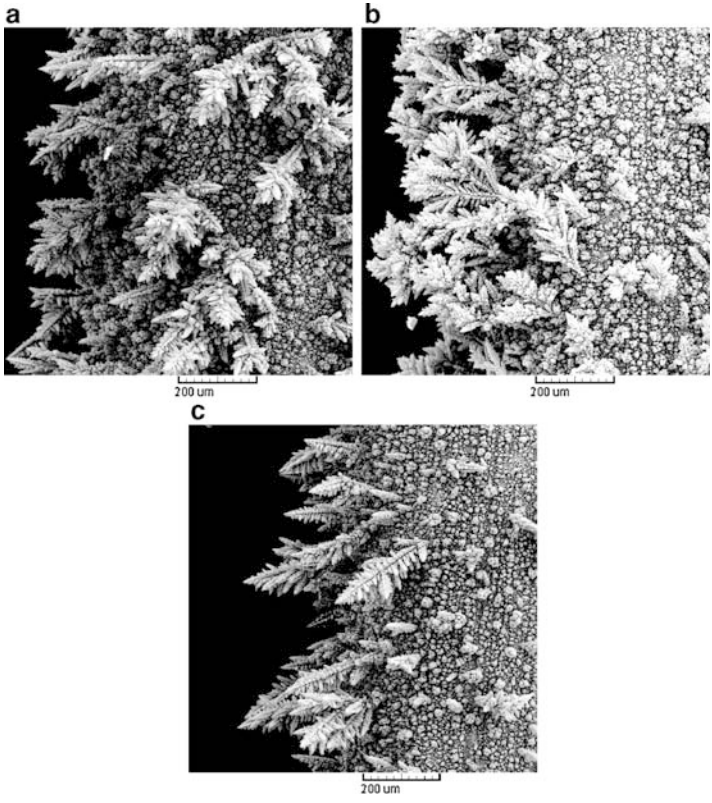

Figure 33. Copper deposits obtained at an overpotential of 650 mV from: (**a**) 0.15 M $CuSO_4$ in 0.125 M H_2SO_4, (**b**) 0.15 M $CuSO_4$ in 0.25 M H_2SO_4, and (**c**) 0.15 M $CuSO_4$ in 1.0 M H_2SO_4. Quantity of electricity: 10 mA h cm^{-2}. (Reprinted from Ref. [67] with permission from Elsevier).

the obtained values of the average current efficiencies of hydrogen evolution in the dependence of concentration of H_2SO_4 at overpotentials of 650, 800, and 1,000 mV[60,67] are given in Table 2. For all examined solutions, overpotentials of 550 and 650 mV corresponded to the plateau of the limiting diffusion current density, while overpotentials of 800 and 1,000 mV were about 50 and 250 mV outside the plateau of the limiting diffusion current density, respectively (Fig. 32).

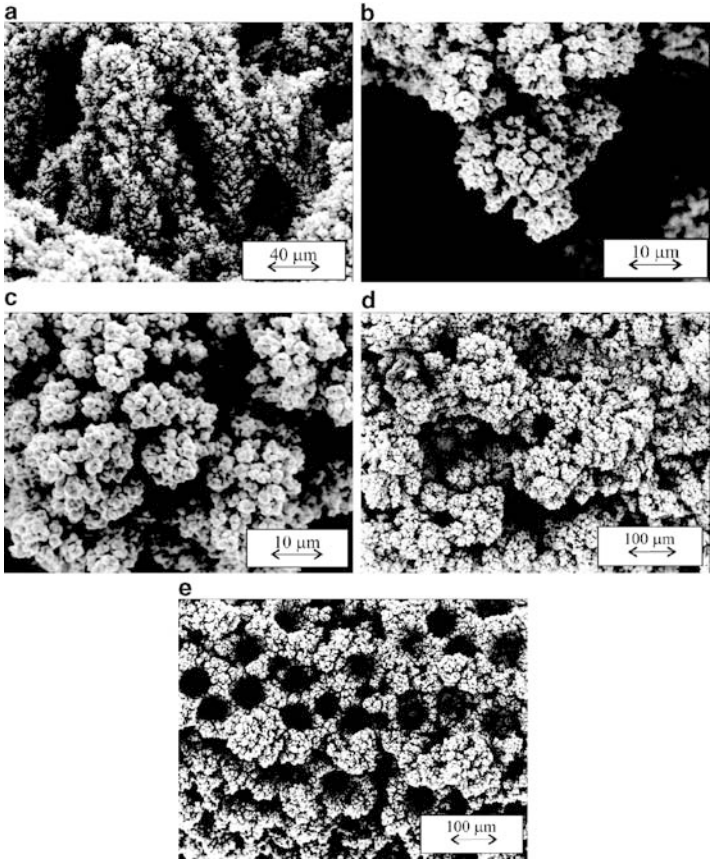

Figure 34. Copper deposits obtained at an overpotential of 800 mV from: (**a–c**) 0.15 M $CuSO_4$ in 0.125 M H_2SO_4; (**d**) 0.15 M $CuSO_4$ in 0.25 M H_2SO_4, and (**e**) 0.15 M $CuSO_4$ in 1.0 M H_2SO_4. Quantity of electricity: 10 mA h cm^{-2}. (Reprinted from Ref. [60] with permission from Elsevier).

(i) Morphologies of Copper Deposits Obtained at Overpotentials up to 800 mV

Electrodeposition of copper at an overpotential of 550 mV from 0.15 M $CuSO_4$ in 0.125 M H_2SO_4, as well as from 0.15 M $CuSO_4$ in 0.25 M H_2SO_4 led to the formation of dendritic forms with the quantity of the electricity of 10 mA h cm^{-2}.[67] The number of copper

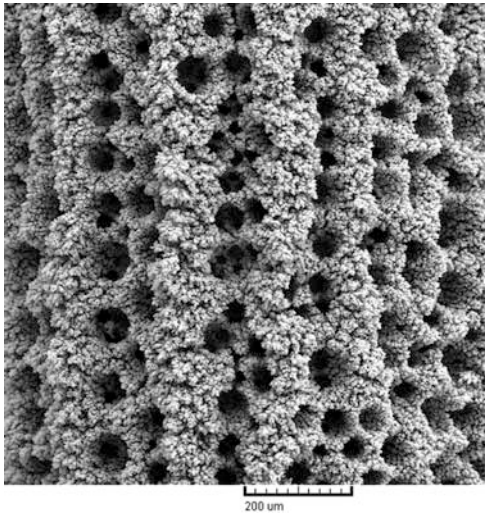

Figure 35. The copper deposit obtained at an overpotential of 1,000 mV from 0.15 M $CuSO_4$ in 1.0 M H_2SO_4. Quantity of electricity: 10 mA h cm^{-2}. (Reprinted from Ref. [67] with permission from Elsevier).

dendrites formed at a surface area of copper electrodes increased with the decrease of the H_2SO_4 concentration. Cauliflower-like forms were obtained by electrodeposition at the same overpotential from 0.15 M $CuSO_4$ in 1.0 M H_2SO_4 with the quantity of the electricity of 10 mA h cm^{-2}. Some of them were developed in dendritic forms by the electrodeposition with the double quantity of electricity.

Copper dendrites were formed by electrodeposition processes at an overpotential of 650 mV from all three solutions (Fig. 33). It can be seen from Fig. 33 that the number of formed dendritic forms increased with the decrease of H_2SO_4 concentration. Also, the branching of these forms increased with the decrease of the concentration of H_2SO_4. The corncob-like forms were grouped in flower-like or tree-like forms, or even formed individually at an electrode surface (Fig. 33).

The analysis of copper electrodeposition processes at overpotentials of 550 and 650 mV has shown that the decrease of H_2SO_4 concentration led to the shift of the formation of dendritic forms

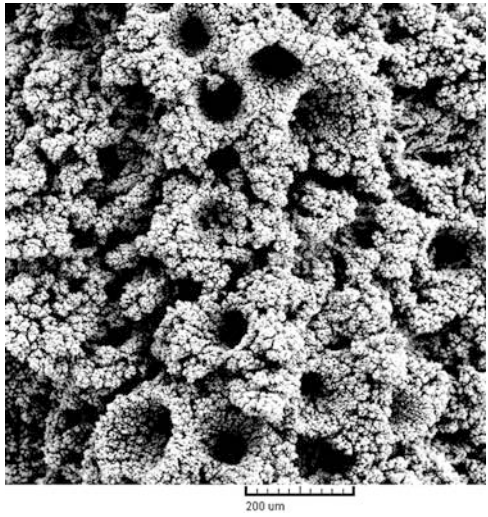

Figure 36. The copper deposit obtained at an overpotential of 1,000 mV from 0.15 M $CuSO_4$ in 0.25 M H_2SO_4. Quantity of electricity: 10 mA h cm^{-2}. (Reprinted from Ref. [67] with permission from Elsevier).

toward higher overpotentials of electrodeposition. This effect was the same as the one which had been noticed in case of the increasing concentration of Cu(II) ions,[19] as it was discussed considering minimum overpotential for dendritic growth initiation.

The morphologies of the copper deposits obtained at an overpotential of 800 mV are presented in Fig. 34. A channel structure (Fig. 34a), degenerate dendrites (Fig. 34b), and cauliflower-like forms (Fig. 34c) were formed by copper electrodeposition from 0.15 M $CuSO_4$ in 0.125 M H_2SO_4. Holes originating from attached hydrogen bubbles were formed by electrodeposition from 0.15 M $CuSO_4$ in 0.25 M H_2SO_4 (Fig. 34d). Degenerate dendrites and cauliflower-like forms, similar to those shown in Fig. 34b, c, were also formed by electrodeposition from this solution. Finally, the honeycomb-like structure, constructed from holes formed due to attached hydrogen bubbles and cauliflower-like agglomerates of copper grains between them, was formed by the electrodeposition from 0.15 M $CuSO_4$ in 1.0 M H_2SO_4 (Fig. 34e).

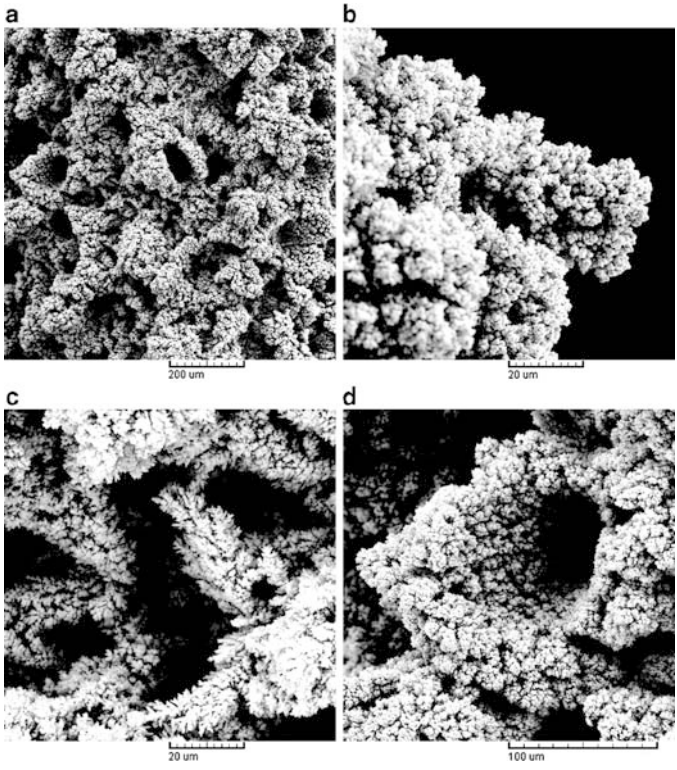

Figure 37. (**a**) The copper deposit obtained at an overpotential of 1,000 mV from 0.15 M $CuSO_4$ in 0.125 M H_2SO_4. Quantity of electricity: 10 mA h cm^{-2}, (**b–d**) details from Fig. 37a: (**b**) degenerate dendrite, (**c**) irregular channels, and (**d**) the shoulder of the hole. (Reprinted from Ref. [67] with permission from Elsevier).

Table 2.
The average current efficiencies of hydrogen evolution in the function of H_2SO_4 concentration. (Reprinted from Refs. [60,67] with permissions from Elsevier).

	The average current efficiencies of hydrogen evolution, $\eta_{av}(H_2)$ (in %), at overpotentials of:		
Solution for copper Electrodeposition	650 mV	800 mV	1,000 mV
0.15 M $CuSO_4$ in 0.125 M H_2SO_4	0	4.83	20.3
0.15 M $CuSO_4$ in 0.25 M H_2SO_4	0.32	9.05	26.4
0.15 M $CuSO_4$ in 1.0 M H_2SO_4	3.3	23.3	45.7

(ii) Morphologies of Copper Deposits Obtained at an Overpotential of 1,000 mV

Morphologies of copper deposits obtained at an overpotential of 1,000 mV from these copper solutions are shown in Figs. 35–37. The honeycomb-like structure was formed by the electrodeposition from 0.15 M $CuSO_4$ in 1.0 M H_2SO_4(Fig. 35). From Fig. 35 it can be seen that holes were lined up in parallel rows. The average diameter of formed holes was 50 μm, while the number of formed holes was 71/mm^2 surface area of the copper electrode.

The honeycomb-like structure was also formed by electrodeposition at 1,000 mV from 0.15 M $CuSO_4$ in 0.25 M H_2SO_4 (Fig. 36). However, in contrast to parallely lined up holes formed from 0.15 M $CuSO_4$ in 1.0 M H_2SO_4, holes which made this honeycomb-like structure were random oriented at the electrode surface. The number of the formed holes was 14/mm^2 surface area of the copper electrode and it was about five times smaller than the number of holes formed from 0.15 M $CuSO_4$ in 1.0 M H_2SO_4. The decrease of concentration of H_2SO_4 led to the increase of the diameter of holes, and the average diameter of holes formed from this solution was estimated to be about 110 μm.

The random-oriented holes were also formed during copper electrodeposition at 1,000 mV from 0.15 M $CuSO_4$ in 0.125 M H_2SO_4 (Fig. 37a). However, the detailed analysis of the copper deposit shown in Fig. 37a revealed the presence of morphological forms which were not obtained by electrodeposition processes from 0.15 M $CuSO_4$ in both 0.25 M and 1.0 M H_2SO_4. Aside from holes and cauliflower-like agglomerates of copper grains between them, the presence of degenerate dendrites (Fig. 37b) and irregular channels formed by evolved hydrogen around dendritic and cauliflower-like particles (Fig. 37c) were also noticed by the analysis of the copper deposit electrodeposited from 0.15 M $CuSO_4$ in 0.125 M H_2SO_4. Additionally, degenerate dendrites were formed at the shoulders of some of holes (Fig. 37d). The average diameter of the formed holes was 120 μm, while their number was estimated to be 7/mm^2 surface area of the copper electrode.

4. The Effect of Temperature on Electrodeposition of Disperse Copper Deposits

The polarization curves for the electrodeposition of copper from 0.15 M $CuSO_4$ in 0.50 M H_2SO_4 at temperatures of 14.0 ± 0.5, 35.0 ± 0.5 and 50.0 ± 0.5°C are given in Fig. 38. It can be seen from Fig. 38 that increasing the temperature leads to an increase of the limiting diffusion current density, as well as to a shift of both the beginning and the end of the plateau of the limiting diffusion current density toward lower electrodeposition overpotentials.

It is clear from Fig. 38 that an overpotential of 550 mV belongs to the plateau of the limiting diffusion current density at all analyzed temperatures. An overpotential of 650 mV belongs to the plateau of the limiting diffusion current density only at a temperature of 14.0 ± 0.5°C. This overpotential is about 50 mV outside the plateau at a temperature of 35.0 ± 0.5°C and about 100 mV outside at a

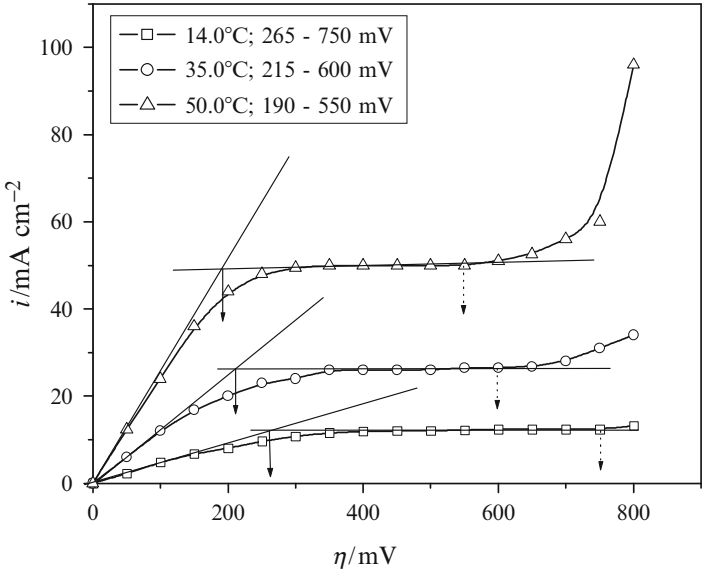

Figure 38. Polarization curves for curves for electrodeposition of copper from 0.15 M $CuSO_4$ in 0.50 M H_2SO_4 at temperatures of 14.0±0.5°C, 35.0±0.5°C, and 50.0 ± 0.5°C. (Reprinted from Ref. [68] with permission from the Serbian Chemical Society).

Table 3.
The values of the average current efficiencies of hydrogen evolution, $\eta_{av}(H_2)$ (in %) in the dependence on temperature of electrodeposition. (Reprinted from Ref. [68] with permission from the Serbian Chemical Society).

	The average current efficiencies of hydrogen evolution, $\eta_{av}(H_2)$ (in %), at overpotentials of:		
Temperature (°C)	550 mV	650 mV	800 mV
14.0 ± 0.5	0	1.6	11.1
35.0 ± 0.5	0	2.2	14.2
50.0 ± 0.5	0	3.7	18.6

temperature of 50.0 ± 0.5°C. Finally, an overpotential of 800 mV is outside the plateau of the limiting diffusion current density at all temperatures.

The average current efficiences for hydrogen evolution reaction, $\eta_{av}(H_2)$, at overpotentials of 650 and 800 mV are summarized in Table 3,[68] which also includes the values of the average current efficiences of hydrogen evolution of 0.0% obtained at an overpotential of 550 mV. It can be clearly seen from Table 3 that the electrodeposition processes at overpotentials of 650 and 800 mV are accompanied by the increase of the average current efficiencies of hydrogen evolution with increasing temperature, causing a shift of the end of the limiting diffusion current density plateau toward lower values of the overpotential. This is due to the increased rate of hydrogen evolution with increasing temperature. In totality, the three groups of the average current efficiences of hydrogen evolution are of significance in the investigation of the effect of temperture on the electrodeposition of copper at high overpotentials.

The first group is characterized by electrodeposition of copper at an overpotential of 550 mV, (potential at which there is no hydrogen evolution or hydrogen evolution was below the sensitivity of the measurement technique).

The second group is characterized by processes of electrodeposition at an overpotential of 650 mV (potential at which the average

current efficiencies of hydrogen evolution were below the critical value of the average current efficiency of hydrogen evolution of 10.0%, leading to a change of the hydrodynamic conditions in the near-electrode layer in this solution).

Finally, the third group includes electrodeposition processes at 800 mV, which are accompanied by an average current efficiency of hydrogen evolution above the critical value of 10.0%.

The morphologies of the copper deposits electrodeposited at an overpotential of 550 mV are cauliflower-like and dendritic ones.[68] The size of the cauliflower-like particles did not change with increasing temperature, but the size of sub-particles constituting the cauliflower-like forms which decreased with increasing temperature of electrodeposition. The decrease of the size of sub-particles with increasing temperature can be explained by the well-known dependence of the nucleation rate on temperature,[69] which was derived by Volmer and Weber.[70]

The morphologies of the copper deposits obtained at an overpotential of 650 mV are shown in Fig. 39, from which the strong effect of temperature on the electrodeposition of copper at an overpotential of 650 mV can immediately be clearly seen. Very branched copper dendrites were formed during electrodeposition at a temperature of 14.0°C (Fig. 39a). They were constructed of corncob-like elements (Fig. 39b). This is in accordance with the position of an overpotential of 650 mV in the limiting diffusion current density plateau. Dendritic forms were obtained during electrodeposition at a temperature of 35.0°C (Fig. 39c) but holes, the origin of which was attached hydrogen bubbles, were also formed (the part in the circle in Fig. 39d). The increased hydrogen evolution at a temperature of 50.0°C compared to that at 35.0°C led to a change of the shape of the copper dendrites, which become similar to cauliflower-like forms (Fig. 39e) or, probably, degenerate dendrites were formed. Also, the holes formed due to the attachment of hydrogen bubbles can be observed in this copper deposit (Fig. 39f). These facts were unexpected because the current efficiency of the hydrogen evolution reaction was lower than 10.0%, but it can be explained by the findings of Vogt and Balzer.[71] They showed that the bubble coverage of an electrode surface increased with temperature more than linearly. Besides, Krenz[72] observed an increase in bubble coverage of about 50% as the temperature was raised from 25 to 50°C.

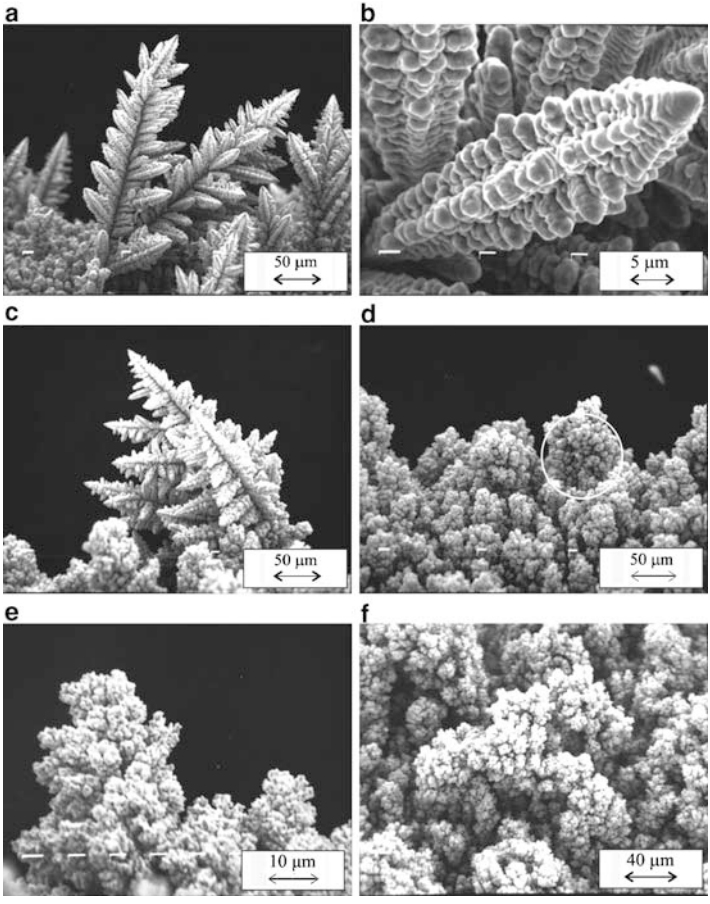

Figure 39. Morphologies of copper deposits electrodeposited at an overpotential of 650 mV at temperatures of: (**a, b**) 14.0 ± 0.5°C, (**c, d**) 35.0 ± 0.5°C, and (**e, f**) 50.0 ± 0.5°C. (Reprinted from Ref. [68] with permission from the Serbian Chemical Society).

The morphologies of the copper deposits electrodeposited at an overpotential of 800 mV are shown in Fig. 40, from which the strong effect of evolved hydrogen on the morphologies of copper deposits is visible. Very porous structures, holes formed due to the attachment of hydrogen bubbles, cauliflower-like forms, and the absence

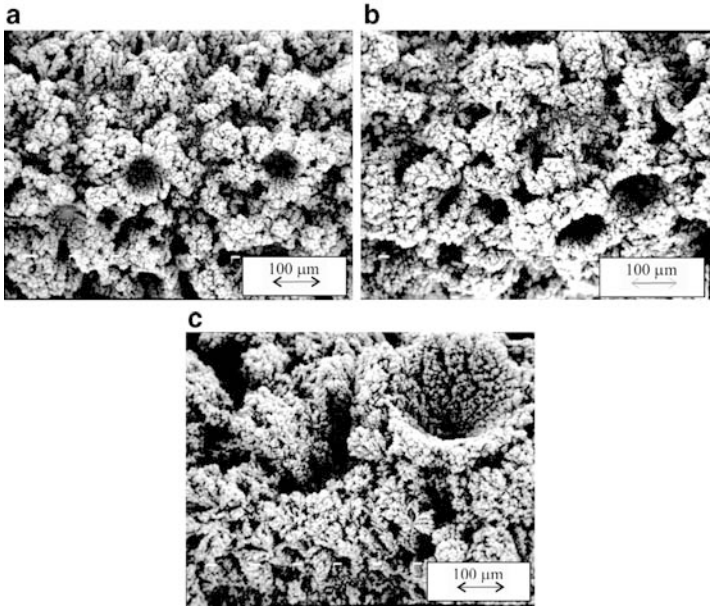

Figure 40. Morphologies of copper deposits electrodeposited at an overpotential of 800 mV at temperatures of: (**a**) $14.0 \pm 0.5°C$, (**b**) $35.0 \pm 0.5°C$, and (**c**) $50.0 \pm 0.5°C$. (Reprinted from Ref. [68] with permission from the Serbian Chemical Society).

of dendritic forms were the main characteristics of copper deposits obtained at this overpotential. A decreased number of holes per square millimeter surface area of copper electrodes and the increased diameter of the holes with increasing temperature can be observed from Fig. 40. Also, the portions of the copper structure consisting of disperse agglomerates of copper grains, among which irregular channels were formed, increased with increasing temperature of the solution.

First, it is necessary to note that the decrease of the number of holes per square millimeter surface area of the copper electrode with intensification of hydrogen evolution was very surprising. It is opposed to the already observed phenomena[10,17,18] when it was shown that intensification of hydrogen evolution reaction leads to an increase of the number of holes. Thus, the unexpected development of the copper structures with intensification of the hydrogen

evolution reaction clearly highlights the necessity to take into consideration the effect of temperature on some properties of electroplating solution, as well as the already mentioned increased bubble coverage with the increasing temperature. The properties of an electrolyte of importance in metal electrodeposition processes which are affected by a change of temperature are the viscosity[73] and surface tension of the electrolyte.[71]

In Ref.[68] are given the values of the viscosity and surface tension of a copper solution containing 0.15 M $CuSO_4$ in 0.50 M H_2SO_4 at the examined temperatures. As expected, both the viscosity and the surface tension of this solution decrease with increasing temperature. The decrease of the surface tension of the solution lowers the break-off diameter of hydrogen bubble from the electrode surface,[71] while the decreased viscosity of the solution probably facilitates the transport of the detached hydrogen bubbles through the interior of the deposit, thus forming a channel structure through it. A typical channel structure formed at an overpotential of 800 mV at a temperature of 50.0°C is shown in Fig. 41a, while the top view of this deposit shows that very disperse cauliflower-like agglomerates of copper grains were surrounded by irregular channels (Fig. 41b).

Hence, increase the temperature led to a redistribution of evolved hydrogen from those creating a honeycomb-like structure (holes formed due to the attachment of hydrogen bubbles with cauliflower-like agglomerates of copper grains between them) to those making a copper structure with the dominant presence of cauliflower-like forms and irregular channels between them.

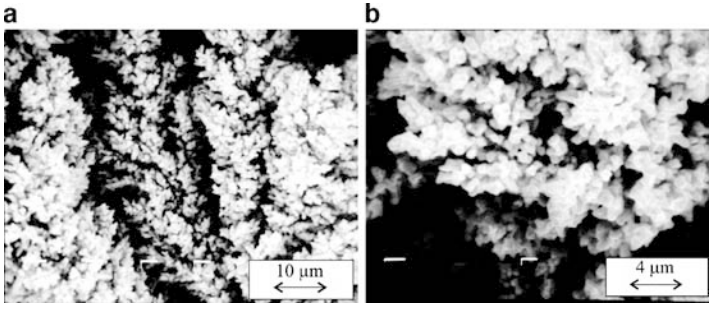

Figure 41. Morphologies of copper deposits electrodeposited at an overpotential of 800 mV at a temperature of 50.0 ± 0.5°C: (**a**) the channel structure, and (**b**) the top view of the deposit. (Reprinted from Ref.[68] with permission from the Serbian Chemical Society).

This increase of the portion of channel structure to the overall structure of the deposit in relation to the portion of holes to the overall structure is probably due to changes of the properties of the electroplating solution, caused by the dependences of the viscosity and surface tension of solution on temperature. As a result of this, the formation of holes becomes less possible and hence large holes appear only due to the edge effect, as can be clearly seen from Fig. 40c. It is obvious that the probability of the formation of the nucleus of such a structure decreases with lowering of the break-off diameter of the bubbles.

Also, it is necessary to note that increasing the temperature led to the formation of morphological forms of copper deposits characteristic for electrodeposition at higher overpotentials, probably because of the increase of bubble coverage with increasing temperature. The effect of temperature was opposite to those observed with increasing the concentration of Cu(II) ions,[19] when increasing concentration of Cu(II) ions led to a the formation of morphological forms of copper deposits characteristic for electrodeposition at lower overpotentials.[19]

5. Analysis of Deposition Conditions with the Aspect of the Honeycomb-like Structure Formation

It is obvious that the honeycomb-like structures can be considered as possible electrodes in electrochemical devices such as fuel cells and sensors due to their very open and porous structure. Analysis of the effect of different parameters of electrolysis given in this section enables to be systematized electrodeposition conditions leading to the formation of this structure type.

The acceleration of electrochemical processes through the increase of concentration of Cu(II) ions above 0.15 M $CuSO_4$ (in 0.50 M H_2SO_4) showed an unfavorable effect to the formation of the honeycomb-like structure due to the formation of dish-like holes with the higher concentrations of Cu(II) ions.[58]

The formation of degenerate dendrites (Fig. 37b), a channel structure around dendritic and cauliflower-like particles (Fig. 37c) and holes with the shoulders of degenerate dendrites (Fig. 37d) clearly points out that hydrodynamic conditions in the near-electrode layer were not changed by electrodeposition of copper from 0.15 M $CuSO_4$ in 0.125 M H_2SO_4. This was very surprising having in mind a relatively high average current efficiency of hydrogen evolution

of 20.3% by which this deposit was formed. Anyway, it is very clear that the quantity of evolved hydrogen is not the only parameter responsible for the formation of the honeycomb-like structures, and therefore, the analysis of the composition of electrodeposition solutions and electrodeposition conditions is very important. In order to explain different morphological forms obtained under hydrogen co-deposition, Fritz equation,[74] modified by Stephan,[75] for the bubble break-off diameter at zero current, d_0 will be used.

This bubble break-off diameter, d_0, can be presented by (13):

$$d_0 = 1.20\vartheta\sqrt{\frac{\gamma}{g\,(\rho_L - \rho_G)}} \tag{13}$$

where ϑ is contact angle, γ is surface tension, ρ_L is a density of liquid phase, and ρ_G is a density of gaseous phase.

The bubble break-off diameter depends on a current density and as it was shown by numerous experiments,[71,76,77] it decreases with increasing current density. The fact that break-off diameter decreases with increasing current density is the result of varying electrode potential which affect the wettability and, hence, the contact angle supports the conclusion that (13) is a basic relationship to explain the dependence of the break-off diameter on the current density. Then, the bubble break-off diameter, d can be presented by (14):[71]

$$\frac{d}{d_0} = \left(1 + 0.2\frac{I/S}{\mathrm{Am}^{-2}}\right)^{-0.45} \tag{14}$$

where I/S is the superficial current density.

Using (13) and (14) as well as the fact that a contact angle decreases with lowering surface tension,[78] the formation of morphologies of copper deposits shown in Figs. 35–37 can be considered as follows. In Table 4 are given the values for a density and a surface tension of the examined solutions. As expected,[79] the density of copper solutions increased with the increase of concentration of H_2SO_4, while the increasing concentration of H_2SO_4 lowered the surface tension values of the examined solutions. The use of electroplating solution with lower surface tension generates more hydrogen bubbles during copper electrodeposition,[78] which is definitely confirmed in this investigation. It can be seen from Table 4 that the change of the density and the surface tension with increasing H_2SO_4 concentration was less than 5%.

Table 4.
The values of the density, ρ, and the surface tension, γ, of copper solutions containing 0.15 M $CuSO_4$ in 0.125, 0.25 and 1.0 M H_2SO_4. (Reprinted from Ref. [67] with permission from Elsevier).

Solution for copper Electrodeposition	ρ(kg dm^{-3})	$\gamma \times 10^3$ (J m^{-2})
0.15 M $CuSO_4$ in 0.125 M H_2SO_4	1.033	100.2
0.15 M $CuSO_4$ in 0.25 M H_2SO_4	1.038	98.7
0.15 M $CuSO_4$ in 1.0 M H_2SO_4	1.081	97.6

In order to apply (14) to potentiostatic conditions of electrodeposition, an average current density, I_{av}/S should be taken into consideration. An average current density, I_{av}/S can be presented by (15), and it was shown that the average current density increased with the increasing concentration of H_2SO_4.[67]

$$I_{av}/S = (1/t)\int_0^t i\,dt \tag{15}$$

Hence, according to (13), the increase of a density and the decrease of a surface tension of solution lead to a decrease of the bubble break-off diameter. According to (14) and (15), at the same deposition overpotential, copper electrodeposition by the higher average current density in addition decreases the break-off diameter of hydrogen bubbles. It is very clear from the above consideration that the contribiution of the average current density to the decrease of the break-off diameter is larger than the contribution of the density and the surface tension of the solutions. It can be concluded that the change of the break-off diameter of hydrogen bubbles with the change of H_2SO_4 concentration is consequence of synergetic effect of electroplating solutions properties and electrodeposition conditions. Anyway, the analysis of densities and surface tensions of the examined solutions, as well as the average current densities of electrodeposition successfully explains the change of the size of holes formed under the described hydrogen co-deposition conditions (Figs. 35–37).

Finally, the analysis of the break-off diameter (or the diameter of the detached hydrogen bubble) can give an explanation why the change of hydrodynamic conditions in the near-electrode layer is achieved from the copper solution with the lower quantity of evolved hydrogen (i.e. from 0.15 M $CuSO_4$ in 0.50 M H_2SO_4 at 800 mV

with the quantity of evolved hydrogen corresponding to $\eta_{av}(H_2)$ of 10.8%, but not from 0.15 M $CuSO_4$ in 0.125 M H_2SO_4 where the quantity of evolved hydrogen corresponded to $\eta_{av}(H_2)$ of 20.3%).

An increase of the density and the lowering of surface tension of the solution decreases the break-off diameter of bubble ((13) and (14)), and consequently, reduce the time needed for its detachment from an electrode surface. After the detachment of hydrogen bubble, the further electrodeposition process occurs by the formation of new hydrogen bubbles at an energetically active sites of electrode surface. A successive processes of the formation of hydrogen bubbles at an energetically active sites of electrode surface and their ability to relatively fast achieve the critical size for the detachment from electrode surface, produces an sufficient amount of hydrogen bubbles which can cause an effective stirring of solution in the near-electrode layer. This will lead to the decrease of the cathode diffusion layer thickness and the increase of the limiting diffusion current density, and as a result of this, the change of hydrodynamic conditions in the near-electrode layer is achieved. In this way, copper structures constructed of holes and agglomerates of copper grains between them, as well as without dendritic forms (denoted as the honeycomb-like structure) are formed.

On the other hand, the use of an electroplating solution of lower density and higher surface tension increases the break-off diameter of hydrogen bubbles. It means that during electrodeposition process from such a solution, newly formed hydrogen bubbles coalesce primarily with hydrogen bubbles formed in the initial stage of electrodeposition, increasing their diameter and prolonging a time needed for their detachment from electrode surface. In this way, the number of formed hydrogen bubbles will not be sufficient to cause an effective stirring of solution in the near-electrode layer. As a result of insufficient change of hydrodynamic conditions in the near-electrode layer, dendritic growth is not inhibited completely and degenerate dendrites as well as dendritic particles inside channels formed of evolved hydrogen were obtained.

The analysis of a number of holes formed per square millimeter surface area of copper electrodes and the average diameter of holes obtained from 0.15 M $CuSO_4$ in 0.50 M H_2SO_4 at 800 mV and from 0.15 M $CuSO_4$ in 0.125 M H_2SO_4 at 1,000 mV confirms above consideration. The number of holes formed due to the attached hydrogen bubbles from 0.15 M $CuSO_4$ in 0.50 M H_2SO_4 at 800 mV was 10/mm^2 surface area of copper electrode,[17] while their average

diameter was approximately 98.7 μm. This number was for about 40% larger than the number of holes formed from 0.15 M $CuSO_4$ in 0.125 M H_2SO_4 at 1,000 mV. The average diameter of holes formed from 0.15 M $CuSO_4$ in 0.125 M H_2SO_4 at 1,000 mV was for about 20% larger than the average diameter of those formed from 0.15 M $CuSO_4$ in 0.50 M H_2SO_4 at 800 mV.

Anyway, the results of the performed qualitative consideration clearly indicate that Fritz equation[74] modified by Stephan[75] can be applied for the examination of copper electrodeposition processes under hydrogen co-deposition in potentiostatic conditions.

The acceleration of electrochemical processes through the increase of a temperature of electrolysis showed an unfavorable effect to the formation of the honeycomb-like structures.[68] The increase of a temperature leads to the decrease of number of holes because of the effect of a temperature on some properties of solutions such as a viscosity and a surface tension.[68,71–73]

Hence, the conditions which must be fulfilled in order to get the honeycomb-like structure are: electrodeposition from the solutions with lower concentrations of Cu(II) ions (0.15 M $CuSO_4$ and less) in a concentration range from 0.25 M to 1.0 M H_2SO_4, at a temperature of 18.0 $\pm$ 1.0°C and at overpotentials outside the plateau of the limiting diffusion current density at which hydrogen evolution is vigorous enough to change hydrodynamic conditions in the near-electrode layer. The critical quantity of evolved hydrogen enabling the formation of the honeycomb-like structures under the given electrodeposition conditions corresponds to the average current efficiency of hydrogen evolution, $\eta_{av}(H_2)$ of 10.0%.[19]

The number of craters or holes forming the honeycomb-like structure increased rapidly with the quantity of evolved hydrogen, as can be seen from Fig. 42 which shows the dependence of the number of holes or craters formed due to the attachment of hydrogen bubbles on the average current efficiency of hydrogen evolution.

V. INFLUENCE OF IONIC EQUILIBRIUM IN THE $CuSO_4$–H_2SO_4–H_2O SYSTEM ON THE FORMATION OF IRREGULAR ELECTRODEPOSITS OF COPPER

The most suitable way to analyze the ionic equilibrium in the $CuSO_4$–H_2SO_4–H_2O system was the examination of electrodeposition processes at overpotentials outside the plateau of the

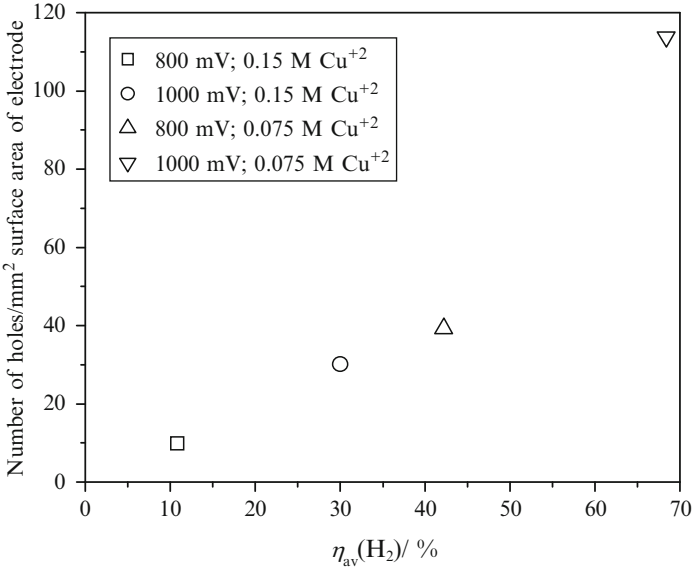

Figure 42. The dependence of the number of holes formed due to the attachment of hydrogen bubbles per square millimeter surface area of copper electrode on the average current efficiency of hydrogen evolution. (Reprinted from Ref. [19] with permission from MDPI).

limiting diffusion current density, due to the hydrogen evolution reaction which occurs parallel to the copper electrodeposition. In order to do it, two sets of acid sulfate solutions were analyzed. In one set of experiments, the concentration of $CuSO_4$ was the same (0.15 M $CuSO_4$), while the concentration of H_2SO_4 was different (0.125, 0.25, and 1.0 M H_2SO_4). The other set of experiments was performed with a constant concentration of H_2SO_4 and different concentrations of $CuSO_4$ (0.075, 0.30, and 0.60 M $CuSO_4$ in 0.50 M H_2SO_4). Then, the volumes of the evolved hydrogen (calculated as the average current efficiencies of hydrogen evolution) and the morphologies of copper deposits obtained at an overpotential of 800 mV for the same ratio of $CuSO_4/H_2SO_4$ were mutually compared and discussed in terms of the relative concentrations of hydrogen ions (H^+) as a function of the H_2SO_4 concentration.[60]

The ratios $CuSO_4/H_2SO_4$ were: 1.2 (for the copper solutions containing 0.15 M $CuSO_4$ in 0.125 M H_2SO_4 and 0.60 M $CuSO_4$

in 0.50 M H_2SO_4), 0.60 (for the copper solutions containing 0.15 M $CuSO_4$ in 0.25 M H_2SO_4 and 0.30 M $CuSO_4$ in 0.50 M H_2SO_4), and 0.15 (for the copper solutions containing 0.15 M $CuSO_4$ in 1.0 M H_2SO_4 and 0.075 M $CuSO_4$ in 0.50 M H_2SO_4).[60]

Analyzing the $CuSO_4/H_2SO_4$ ratio of 1.2 by insight into the ionic equilibrium of the species in the $CuSO_4$–H_2SO_4–H_2O system (Fig. 1), where the position of the Cu concentration of 0.15 M can easily be calculated, it can be noticed that the relative concentration of H^+ ions is larger for the copper solution containing 0.15 M $CuSO_4$ in 0.125 M H_2SO_4 than it is for the one containing 0.60 M $CuSO_4$ in 0.50 M H_2SO_4. This is confirmed by the larger average current efficiency of hydrogen evolution from 0.15 M $CuSO_4$ in 0.125 M H_2SO_4 (4.83%) than from 0.60 M $CuSO_4$ in 0.50 M H_2SO_4 (0.66%). The obtained morphologies of the copper deposits (Figs. 34a–c and 25e) also were in a good agreement with the determined average current efficiency of hydrogen evolution and this ionic equilibrium. The formation of degenerate dendrites from 0.15 M $CuSO_4$ in 0.125 M H_2SO_4 is the consequence of the larger quantity of evolved hydrogen from this solution than from 0.60 M $CuSO_4$ in 0.50 M H_2SO_4 when copper dendrites only were formed.

A similar consideration can also be applied to the $CuSO_4/H_2SO_4$ ratio of 0.60. According to the ionic equilibrium in $CuSO_4$–H_2SO_4–H_2O system, the relative concentration of H^+ ions is larger for a copper solution containing 0.15 M $CuSO_4$ in 0.25 M H_2SO_4 than for one containing 0.30 M $CuSO_4$ in 0.50 M H_2SO_4. The experimentally determined average current efficiency of hydrogen evolution and the observed morphologies of the copper deposits (Figs. 34d and 25b–d) were also in good agreement with the calculation of this ionic equilibrium. The presence of dendritic forms during electrodeposition from 0.30 M $CuSO_4$ in 0.50 M H_2SO_4 at 800 mV (Fig. 25b) clearly indicates that copper electrodeposition was accompanied by a smaller quantity of evolved hydrogen from this solution than from 0.15 M $CuSO_4$ in 0.25 M H_2SO_4.

Finally, the honeycomb-like copper structures were obtained with a $CuSO_4/H_2SO_4$ ratio of 0.15. The honeycomb-like copper structure was formed from 0.075 M $CuSO_4$ in 0.50 M H_2SO_4 under more vigorous hydrogen evolution than that formed from 0.15 M $CuSO_4$ in 1.0 M H_2SO_4, which is also in agreement with the calculation of the ionic equilibrium in the $CuSO_4$–H_2SO_4–H_2O system.

VI. THE SHAPE OF ELECTROCHEMICALLY FORMED COPPER POWDER PARTICLES AND THEIR DEPENDENCE ON THE QUANTITY OF EVOLVED HYDROGEN

In spite of detailed investigations of the formation and properties of metal powders obtained by electrolysis,[13,22–25] the first report which considered the effect of hydrogen evolution on the shape of powder particles was given recently.[80]

It was found[80] that two types of powder copper particles are formed, depending on the quantity of evolved hydrogen. The first type is formed with a quantity of evolved hydrogen which is insufficient to change the hydrodynamic conditions in the near-electrode layer ($\eta_{av}(H_2) < 10.0\%$), whereas the second type is formed when the quantity of evolved hydrogen is sufficient to change the hydrodynamic conditions in the near-electrode layer ($\eta_{av}(H_2) > 10.0\%$).

The first type of copper powder particles is shown in Fig. 43a. These particles were obtained by tapping the copper deposit obtained by electrodeposition from 0.15 M $CuSO_4$ in 0.50 M H_2SO_4 at an overpotential of 700 mV which was accompanied by $\eta_{av}(H_2)$ of 1.97%.[10] It can be seen from Fig. 43a that the copper particles were highly branched dendrites. The typical branchy from which these powder particles are constructed is presented in Fig. 43b.

The basic element from which this type of powder particles is constructed was obtained by a treatment of the copper powder

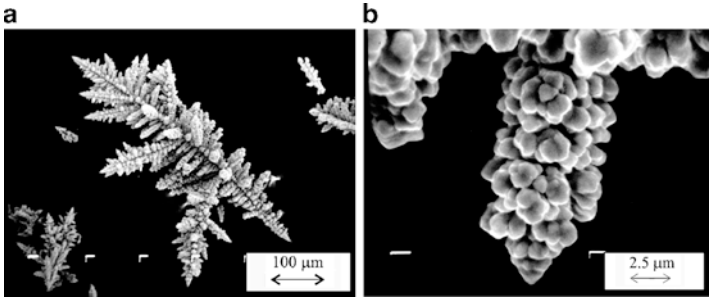

Figure 43. SEM photomicrographs of copper powder particles obtained by electrodeposition from 0.15 M $CuSO_4$ in 0.50 M H_2SO_4, at an overpotential of 700 mV: (**a**) dendritic particle, and (**b**) the detail from Fig. 43a. (Reprinted from Ref. [80] with permission from Elsevier).

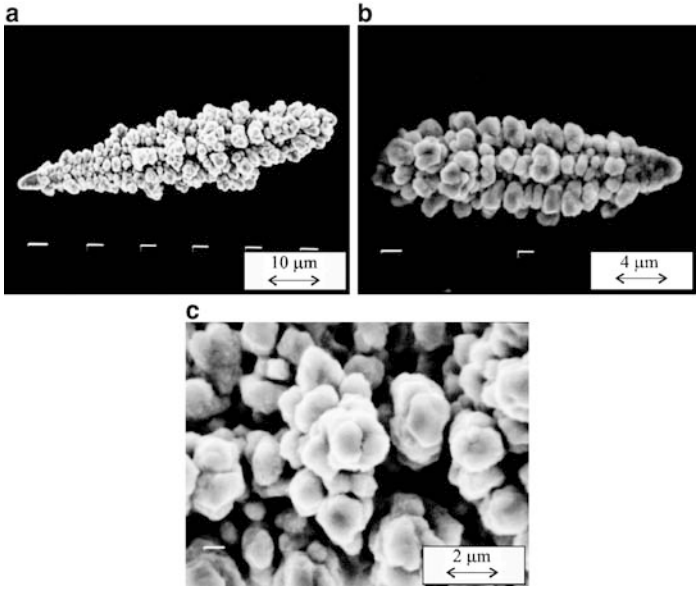

Figure 44. SEM photomicrographs of copper powder particles shown in Fig. 43 after treatment in an ultrasonic field: (**a, b**) the basic elements of the dendritic particles, and (**c**) the micro structure of the basic element. (Reprinted from Ref. [80] with permission from Elsevier).

particles shown in Fig. 43 in an ultrasonic field. The resulting particles are shown in Fig. 44. From Fig. 44a, b, it can be seen that the particles obtained had a corncob-like structure. They all took the form of branches of dendrites but, although they had the same surface structure, a difference in their size was noticeable. Analysis of these branches at the micro level revealed that the branches consisted of agglomerates of copper grains (Figs. 43b and 44c).

According to Wranglen,[81] a dendrite consists of a stalk and branches (primary, secondary, etc.). It is obvious from Figs. 43 and 44 that the corncob-like elements forming the branches constitute the dendritic character of these particles. These corncob-like elements can be grouped in different forms of dendritic particles or alternatively can be formed individually at the electrode surface. This can easily be seen from Fig. 45, which shows disperse deposits immediately before they were tapped from the electrode surface. They were all obtained by electrodeposition processes when the

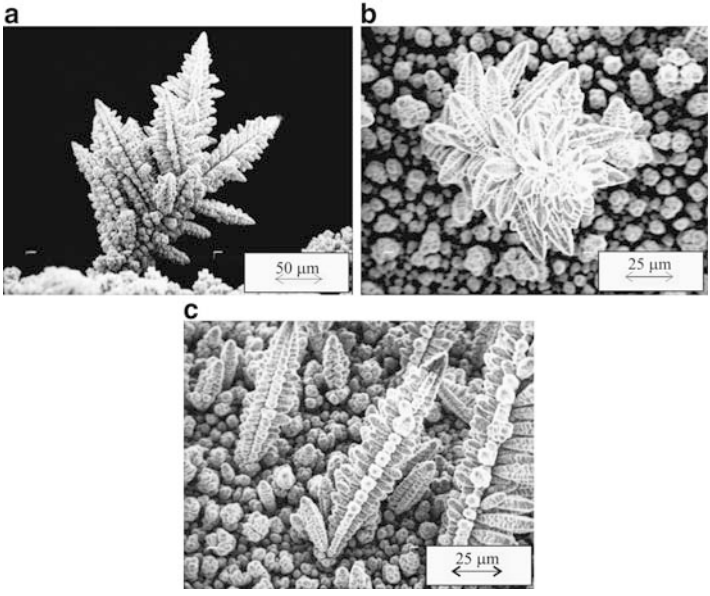

Figure 45. SEM photomicrographs of the copper powder deposits obtained by electrodeposition at an overpotential of 650 mV from: (**a**) 0.075 M $CuSO_4$ in 0.50 M H_2SO_4; (**b, c**) 0.30 M $CuSO_4$ in 0.50 M H_2SO_4. (Reprinted from Ref. [80] with permission from Elsevier).

quantities of evolved hydrogen were below the critical value for a change in the hydrodynamic conditions in the near-electrode layer. Figure 45a shows the powder deposit electrodeposited at an overpotential of 650 mV from 0.075 M $CuSO_4$ in 0.50 M H_2SO_4 ($\eta_{av}(H_2)$ was 7.5%),[19] whereas Fig. 45b, c shows the powder deposits electrodeposited at the same overpotential but from 0.30 M $CuSO_4$ in 0.50 M H_2SO_4 ($\eta_{av}(H_2)$ was 0.83%).[19] The electrodeposition process which led to the formation of the highly branched dendritic particles was controlled by the diffusion of ions to the electrode surface, rather than electron transfer control.[13]

The powder particles belonging to the second type are shown in Fig. 46a. They are obtained by tapping the copper deposit electrodeposited from 0.15 M $CuSO_4$ in 0.50 M H_2SO_4 at an overpotential of 1,000 mV at which the electrodeposition of copper was accompanied by vigorous hydrogen evolution, corresponding to

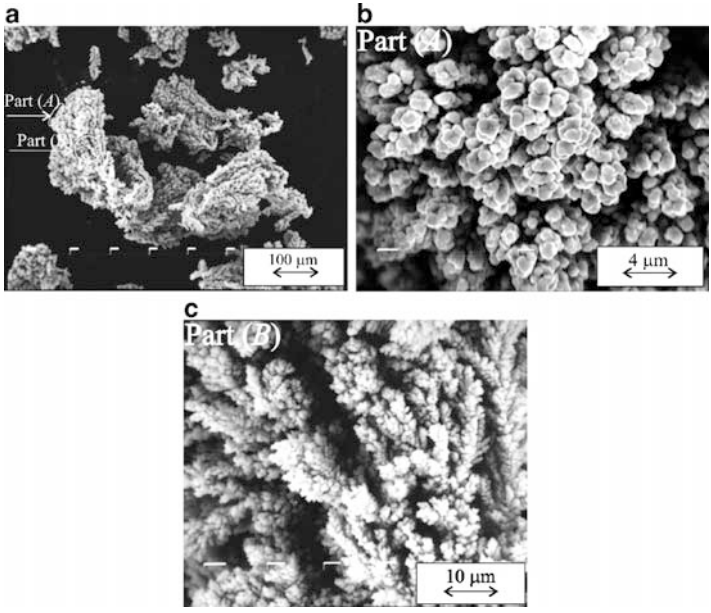

Figure 46. SEM photomicrographs of copper powder particles obtained by electrodeposition from 0.15 M $CuSO_4$ in 0.50 M H_2SO_4, at an overpotential of 1,000 mV: (**a**) sponge-like particle, and (**b, c**) *Part (A)* and *Part (B)* details from Fig. 46a. (Reprinted from Ref. [80] with permission from Elsevier).

$\eta_{av}(H_2)$ of 30.0%.[10] These powder particles were sponge-like and the difference between them and those formed when the quantity of evolved hydrogen was below the critical value for a change in the hydrodynamic conditions (Figs. 43–45) is clear. For this reason, further analysis of these particles is necessary. The parts of the powder particle denoted with *Part* (*A*) and *Part* (*B*) in Fig. 46a are shown at higher magnifications in Fig. 46b, c, respectively. It can be seen from Fig. 46b that these particles actually have a cauliflower-like structure. In Fig. 46c, a porous, channel structure through the interior of the powder particle can be seen. These channels were generated in situ by the simultaneous processes of the formation of copper particles and vigorous hydrogen evolution.

The basic element from which this type of powder particles is constructed was obtained by treatment of the particles shown in Fig. 46a in an ultrasonic field. Figure 47 shows the particles obtained

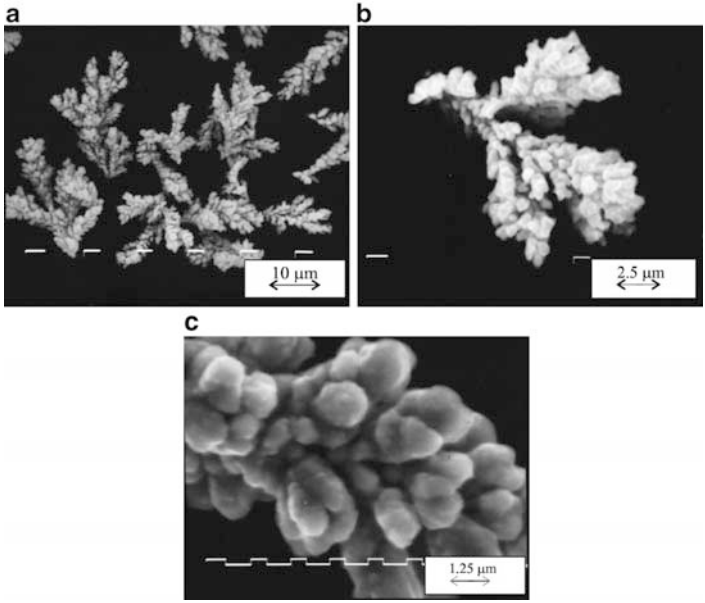

Figure 47. SEM photomicrographs of copper powder particles shown in Fig. 46 after treatment in an ultrasonic field: (**a, b**) the basic elements of the sponge-like particles, and (**c**) the micro structure of the basic element. (Reprinted from Ref. [80] with permission from Elsevier).

after treatment in an ultrasonic field. It can be seen that the structure of the basic element of which these powder particles are composed was completely different to that obtained when the amount of evolved hydrogen was below the critical value for a change in the hydrodynamic conditions in the near-electrode layer. In this case, corncob-like structures were not formed. The particles obtained had irregular shapes and had the appearance of degenerate dendrites. This shape is obviously caused by the vigorous hydrogen evolution, or hydrogen stream, which prevents the growth of the copper deposit in one direction, resulting in particles with a curvilinear form. Agglomerates of copper grains can also clearly be seen in these powder particles (Fig. 47b, c).

Although the powder particles obtained with evolved hydrogen below and above the critical value for a change in the hydrodynamic conditions were very different at the macro level, their similarity at the micro level is very clear. Both types of powder particles consisted

of agglomerates of copper grains. The only difference lay in the size of the individual copper grains of which these agglomerates were constituted – that is, the individual copper grains obtained at an overpotential of 1,000 mV were considerably smaller. This difference can be explained by the higher nucleation rate at an overpotential of 1,000 mV than at an overpotential of 700 mV.

The mechanism of electrodeposition of copper under intensive hydrogen evolution is completely different from that which led to the formation of dendritic particles. The quantity of evolved hydrogen corresponding to an average current efficiency of hydrogen evolution of 30.0% was sufficient to cause mixing of the solution in the near-electrode layer, decreasing the cathode diffusion layer thickness and increasing the limiting diffusion current density. The formation of this type of powder particle can be successfully explained by the concept of "effective overpotential."[10]

ACKNOWLEDGMENT

The work was supported by the Ministry of Science and Technological Development of the Republic of Serbia under the research project: "Deposition of ultrafine powders of metals and alloys and nanostructured surfaces by electrochemical techniques" (No. 142032G).

REFERENCES

[1]H.-C. Shin, J. Dong, and M. Liu, *Adv. Mater*. **15** (2003) 1610.
[2]D. R. Gabe, *J. Appl. Electrochem*. **27** (1997) 908.
[3]J. K. Dennis and T. E. Such, *Nickel and Chromium Plating*, Newnes–Butterworths, London (1972).
[4]R. Weiner and A. Walmsley, *Chromium Plating*, Finishing Publications Ltd., Teddington, Middlesex, England (1980).
[5]F. A. Lowenheim, *Electroplating,* McGraw-Hill Book Company, New York; St. Louis (1978).
[6]T. J. Wolery, *EQ3NR – A Computer Program for Geochemical Aqueous Speciation-Solubility Calculations: Theoretical Manual and User'guide, Version 7.0*. Lawrence Livermore National Laboratory, Livermore, CA (1992).
[7]A. Roine, *HSC Chemistry: Chemical Reaction and Equilibrium Software with Extensive Thermochemical Database. 4.0*. Outokumpu Research Oy, Finland (1999).
[8]J. M. Casas, F. Alvarez, and L. Cifuentes, *Chem. Eng. Sci*. **55** (2000) 6223.

[9]K. S. Pitzer, *Activity Coefficients in Electrolyte Solutions*, 2nd edition, CRC, Boca Raton, FL (1991).
[10]N. D. Nikolić, K. I. Popov, Lj. J. Pavlović, and M. G. Pavlović, *J. Electroanal. Chem*. **588** (2006) 88.
[11]V. D. Jović, B. M. Jović, and M. G. Pavlović, *Electrochim. Acta* **51** (2006) 5468.
[12]V. D. Jović, B. M. Jović, V. Maksimović, and M. G. Pavlović, *Electrochim. Acta* **52** (2007) 4254.
[13]K. I. Popov, S. S. Djokić, and B. N. Grgur, *Fundamental Aspects of Electrometallurgy,* Kluwer Academic/Plenum Publishers, New York (2002), and references therein.
[14]H. Vogt, *J. Appl. Electrochem*. **25** (1995) 764.
[15]J. Eigeldinger, and H. Vogt, *Electrochim. Acta* **45** (2000) 4449.
[16]H. Vogt, *Electrochim. Acta* **50** (2005) 2073.
[17]N. D. Nikolić, K. I. Popov, Lj. J. Pavlović, and M. G. Pavlović, *Surf. Coat. Technol*. **201** (2006) 560.
[18]N. D. Nikolić, K. I. Popov, Lj. J. Pavlović, and M. G. Pavlović, *J. Solid State Electrochem*. **11** (2007) 667.
[19]N. D. Nikolić, K. I. Popov, Lj. J. Pavlović, and M. G. Pavlović, *Sensors* **7** (2007) 1.
[20]G. E. Dima, A. C. A. de Vooys, and M. T. M. Koper, *J. Electroanal. Chem*. **554–555** (2003) 15.
[21]D. Pletcher and Z. Poorbedi, *Electrochim. Acta* **24** (1979) 1253.
[22]A. Calusaru, *Electrodeposition of Metal Powders*, Elsevier Scientific Publishing Company, Amsterdam; Oxford; New York (1979) 296.
[23]K. I. Popov and M. G. Pavlović, in *Modern Aspects of Electrochemistry*, Vol. 24, Ed. by R. W. White, J. O'M. Bockris, and B. E. Conway, Plenum Press, New York (1993) 299–391.
[24]N. D. Nikolić, S. B. Krstić, Lj. J. Pavlović, M. G. Pavlović, and K. I. Popov, "The Mutual Relation of Decisive Characteristics of Electrolytic Copper Powder and Effect of Deposition Conditions On Them", in *Electroanalytical Chemistry Research Trends*, Ed. by K. Hayashi, NOVA Publishers (2009) Chap. 8, 185–209.
[25]M. G. Pavlović and K. I. Popov (2005). *Metal Powder Production by Electrolysis*, Electrochemistry Encyclopedia, http://electrochem.cwru.edu/ed/encycl/art-p04-metalpowder.htm.
[26]M. G. Pavlović, N. D. Nikolić, and K. I. Popov, *J. Serb. Chem. Soc*. **68** (2003) 649.
[27]J. O'M. Bockris, Z. Nagy, and D. Dražić, *J. Electrochem. Soc*. **120** (1973) 30.
[28]K. I. Popov, M. D. Maksimović, J. D. Trnjančev, and M. G. Pavlović, *J. Appl. Electrochem*. **11** (1981) 239.
[29]N. Ibl, *Chemie Ing. Techn*. **33** (1961) 69.
[30]N. Ibl, *Chemie Ing. Techn*. **35** (1963) 353.
[31]L. J. Jenssen and J. G. Hoogland, *Electrochim. Acta* **15** (1970) 1013.
[32]J. O'M. Bockris, A. K. N. Reddy, and M. Gamboa-Aldeco, *Modern Electrochemistry 2A, Fundamentals of Electrodics*, Kluwer Academic/Plenum Publishers, New York, 2nd edition (2000).
[33]L. Martins, J. I. Martins, A. S. Romeira, M. E. Costa, J. Costa, and M. Bazzaoui, *Mater. Sci. Forum* **455–456** (2004) 844.
[34]N. D. Nikolić, H. Wang, H. Cheng, C. Guerrero, E. V. Ponizovskaya, G. Pan, and N. Garcia, *J. Electrochem. Soc*. **151** (2004) C577.
[35]N. D. Nikolic, H. Wang, H. Cheng, C. A. Guerrero, and N. Garcia, *J. Magn. Magn. Mater*. **272–276** (2004) 2436.
[36]N. D. Nikolić, *J. Serb. Chem. Soc*. **70** (2005) 1213.
[37]N. D. Nikolić, *J. Serb. Chem. Soc*. **70** (2005) 785.
[38]N. D. Nikolić, *J. Serb. Chem. Soc*. **71** (2006) 1083.

[39]N. D. Nikolić, *J. Serb. Chem. Soc*. **72** (2007) 787.
[40]M. G. Pavlović, Š. Kindlova, and I. Roušar, *Electrochim. Acta* **37** (1992) 23.
[41]R. Aogaki, K. Fueki, and T. Mukaibo, *Denki Kagaku* **43** (1975) 509.
[42]J. P. Glas and J. W. Westwater, *Int. J. Heat Mass Transf*. **7** (1964) 1427.
[43]R. Kaishew and B. Mutafctschiew, *Electrochim. Acta* **10** (1965) 643.
[44]S. Štrbac, Z. Rakočević, K. I. Popov, M. G. Pavlović, and R. Petrović, *J. Serb. Chem. Soc*. **64** (1999) 483.
[45]I. Markov, A. Boynov, and S. Toshev, *Electrochim. Acta* **18** (1973) 377.
[46]K. I. Popov, B. N. Grgur, E. R. Stojilković, M. G. Pavlović, and N. D. Nikolić, *J. Serb. Chem. Soc*. **62** (1997) 433.
[47]A. Milchev, W. S. Kruijt, M. Sluyters-Rehbach, and J. H. Sluyters, *J. Electroanal. Chem*. **362** (1993) 21.
[48]W. S. Kruijt, M. Sluyters-Rehbach, J. H. Sluyters, and A. Milchev, *J. Electroanal. Chem*. **371** (1994) 13.
[49]N. Kovarskii and A. V. Lisov, *Elektrokhimiya* **20** (1984) 221 (in Russian).
[50]N. Kovarskii and A. V. Lisov, *Elektrokhimiya* **20** (1984) 833 (in Russian).
[51]N. Kovarskii and T. A. Arzhanova, *Elektrokhimiya* **20** (1984) 452 (in Russian).
[52]K. I. Popov, Lj. J. Pavlović, M. G. Pavlović, and M. I. Čekerevac, *Surf. Coat. Technol*. **35** (1988) 39.
[53]K. I. Popov, M. G. Pavlović, Lj. J. Pavlović, M. I. Čekerevac, and G. Ž. Remović, *Surf. Coat. Technol*. **34** (1988) 355.
[54]K. I. Popov, M. G. Pavlović, E. R. Stojilković, and Z. Ž. Stevanović, *Hydrometallurgy* **46** (1997) 321.
[55]K. I. Popov, S. K. Zečević, and S. M. Pešić, *J. Serb. Chem. Soc*. **61** (1996) 583.
[56]K. I. Popov, N. D. Nikolić, and Z. Rakočević, *J. Serb. Chem. Soc*. **67** (2002) 635.
[57]K. I. Popov, N. D. Nikolić, and Z. Rakočević, *J. Serb. Chem. Soc*. **67** (2002) 769.
[58]N. D. Nikolić, Lj. J. Pavlović, M. G. Pavlović, and K. I. Popov, *Electrochim. Acta* **52** (2007) 8096.
[59]N. D. Nikolić, Lj. J. Pavlović, G. Branković, M. G. Pavlović, and K. I. Popov, *J. Serb. Chem. Soc*. **73** (2008) 753.
[60]N. D. Nikolić, Lj. J. Pavlović, S. B. Krstić, M. G. Pavlović, and K. I. Popov, *Chem. Eng. Sci*. **63** (2008) 2824.
[61]D. G. Offin, P. R. Birkin, and T. G. Leighton, *Electrochem. Commun*. **9** (2007) 1062.
[62]K. I. Popov, V. Radmilović, B. N. Grgur, and M. G. Pavlović, *J. Serb. Chem. Soc*. **59** (1994) 47.
[63]L. Barton and J. O'M. Bockris, *Proc. R. Soc*. **A268** (1962) 485.
[64]J. W. Diggle, A. R. Despić, and J. O'M. Bockris, *J. Electrochem. Soc*. **116** (1969) 1503.
[65]E. Gileadi, *Electrode Kinetics*, VCH Publishers Inc., New York, (1993) 443.
[66]K. I. Popov, N. V. Krstajić, and M. I. Čekerevac, in: *Modern Aspects of Electrochemistry*, Vol. 30, Ed. by R. E. White, B. E. Conway, and J. O'M. Bockris, Plenum Press, New York (1996) 261–311, and references therein.
[67]N. D. Nikolić, G. Branković, M. G. Pavlović, and K. I. Popov, *J. Electroanal. Chem*. **621** (2008) 13.
[68]N. D. Nikolić, Lj. J. Pavlović, M. G. Pavlović, and K. I. Popov, *J. Serb. Chem. Soc*. **72** (2007) 1369.
[69]E. Budevski, G. Staikov, and W. J. Lorenz, *Electrochemical Phase Formation and Growth, An Introduction to the Initial Stages of metal Deposition*, VCH Weinheim, New York; Basel; Cambridge; Tokyo (1996) 163.
[70]M. Volmer and A. Weber, *Z. Physik. Chem*. **119** (1926) 277.
[71]H. Vogt and R. J. Balzer, *Electrochim. Acta* **50** (2005) 2073.

[72]M. Krenz, *Untersuchung des elektrodennahen Raumes gasentwickelnder elektroden*, Dissertation A, Humboldt-Universitat, Berlin (1984).
[73]A. Amadi, D. R. Gabe, and M. Goodenough, *J. Appl. Electrochem*. **21** (1991) 1114.
[74]W. Fritz, *Phys. Z*. **36** (1935) 379.
[75]K. Stephan, *Heat Transfer in Condensation and Boiling*, Springer, Berlin (1992).
[76]N. Ibl, E. Adam, J. Venczel, and E. Schalch, *Chem. Eng. Tech*. **43** (1971) 202.
[77]H. Vogt, *Gas evolving electrodes*, in: Comprehensive Treatise of Electrochemistry, Vol. 6, Ed. by E. Yeager, J. O. M. Bockris, B. E. Conway, and S. Sarangapani, Plenum Press, New York (1983) 455.
[78]S.-C. Chang, Y.-L. Wang, C.-C. Hung, W.-H. Lee, and G.-J. Hwang, *J. Vac. Sci. Technol. A* **25** (2007) 566.
[79]D. C. Price and W. G. Davenport, *Metall. Trans. B* **11 B** (1980) 159.
[80]N. D. Nikolić, Lj. J. Pavlović, M. G. Pavlović, and K. I. Popov, *Powder Technol*. **185** (2008) 195.
[81]G. Wranglen, *Electrochim. Acta* **2** (1960) 130.